A Novel Shape Memory Polymer (SMP) Foam for Hemorrhage Control

Mary Beth Monroe, Ph.D.
Steven G. Schauer, D.O. MSCR, MAJ USA MC

FINAL REPORT

Date: 15 September 2021

59th Medical Wing
Office of the Chief Scientist
1632 Nellis, BLDG. 5406
JBSA Lackland AFB, TX 78236-7517

DISTRIBUTION A. Approved for public release; distribution is unlimited.

DECLARATION OF INTEREST

The views expressed in this article are those of the authors and do not necessarily reflect the official policy or position of the Department of the Air Force, Department of Defense, nor the U.S. Government. This work was funded by Project Code Number AC12EM01. Authors are military service members, employees, or contractors of the US Government. This work was prepared as part of their official duties. Title 17 USC §105 provides that 'copyright protection under this title is not available for any work of the US Government.' Title 17 USC §101 defines a US Government work as a work prepared by a military service member, employee, or contractor of the US Government as part of that person's official duties.

The views of (manufacturer) are not necessarily the official views of, or endorsed by, the U.S. Government, the Department of Defense, or the Department of the Air Force. No Federal endorsement of (manufacturer) is intended.

NOTICE AND SIGNATURE PAGE

Using Government drawings, specifications, or other data included in this document for any purpose other than Government procurement does not in any way obligate the U.S. Government. The fact that the Government formulated or supplied the drawings, specifications, or other data does not license the holder or any other person or corporation or convey any rights or permission to manufacture, use, or sell any patented invention that may relate to them.

Qualified requestors may obtain copies of this report from the Defense Technical Information Center (DTIC) (http://www.dtic.mil).

A Novel Shape Memory Polymer (SMP) Foam for Hemorrhage Control

TAVISH.MICHELE.F.1031059280 Digitally signed by TAVISH.MICHELE.F.1031059280 Date: 2021.09.29 13:41:24 -05'00'

Michele Tavish, DAF
Program Analyst
En route Care Research Program
59MDW Office of the Chief Scientist

MALLORY.AMBER.MELANIE.1471210206 Digitally signed by MALLORY.AMBER.MELANIE.1471210206 Date: 2021.09.30 15:40:17 -05'00'

Amber Mallory, Ph.D.
Director, Trauma & Clinical Care
59MDW Office of the Chief Scientist

This report is published in the interest of scientific and technical information exchange, and its publication does not constitute the Government's approval or disapproval of its ideas or findings.

REPORT DOCUMENTATION PAGE

Form Approved
OMB No. 0704-0188

1. REPORT DATE *(DD-MM-YYYY)*	2. REPORT TYPE	3. DATES COVERED *(From - To)*
09-09-2021	Final	September 2018-September 2021

4. TITLE AND SUBTITLE

A Novel Shape Memory Polymer (SMP) Foam for Hemorrhage Control

5a. CONTRACT NUMBER

FA8650-18-2-6978

5b. GRANT NUMBER

J917EC06

5c. PROGRAM ELEMENT NUMBER

6. AUTHOR(S)

Monroe, Mary Beth B.
Schauer, Steven G.

5d. PROJECT NUMBER

5e. TASK NUMBER

5f. WORK UNIT NUMBER

7. PERFORMING ORGANIZATION NAME(S) AND ADDRESS(ES)

Syracuse University
318 Bowne Hall
Syracuse NY 13244

8. PERFORMING ORGANIZATION REPORT NUMBER

9. SPONSORING/MONITORING AGENCY NAME(S) AND ADDRESS(ES)

JPC6 Combat Casualty Care Research Program

10. SPONSOR/MONITOR'S ACRONYM(S)

11. SPONSOR/MONITOR'S REPORT NUMBER(S)

12. DISTRIBUTION/AVAILABILITY STATEMENT

UU

13. SUPPLEMENTARY NOTES

14. ABSTRACT

Although there are many hemostatic agents available for use on the battlefield, uncontrolled hemorrhage is still the primary cause of preventable death. Current hemostatic dressings include QuikClot® Combat Gauze (QCCG) and XStat®, which have inadequate success in reducing mortality. To address this need, a new hemostatic material was developed using shape memory polymer (SMP) foams, which demonstrate biocompatibility, rapid clotting, and shape recovery to fill the wound site. SMP foam hemostatic efficacy was examined in a lethal, noncompressible porcine liver injury model over 6 hours following injury. Wounds were packed with SMP foams, XStat, or QCCG and compared in terms of time to bleeding cessation, total blood loss, and animal survival. The hemostatic material properties and in vitro blood interactions were also characterized. SMP foams decreased blood loss and active bleeding time in comparison with XStat and QCCG. Most importantly, SMP foams increased the 6-hour survival rate by 50% and 37% (vs. XStat and QCCG, respectively) with significant increases in survival times. In parallel studies, modifications were made to the foams to make them degradable, which would allow for hemostatic materials to remain in place during healing, and antimicrobial to reduce

15. SUBJECT TERMS

enroute care, hemostatic dressing, hemorrhage control

16. SECURITY CLASSIFICATION OF:			17. LIMITATION OF ABSTRACT	18. NUMBER OF PAGES	19a. NAME OF RESPONSIBLE PERSON
a. REPORT	b. ABSTRACT	c. THIS PAGE			Mary Beth B. Monroe
UU	UU	UU	UU		19b. TELEPHONE NUMBER *(Include area code)* 315-443-3323

ABSTRACT

Although there are many hemostatic agents available for use on the battlefield, uncontrolled hemorrhage is still the primary cause of preventable death. Current hemostatic dressings include QuikClot® Combat Gauze (QCCG) and XStat®, which have inadequate success in reducing mortality. To address this need, a new hemostatic material was developed using shape memory polymer (SMP) foams, which demonstrate biocompatibility, rapid clotting, and shape recovery to fill the wound site. SMP foam hemostatic efficacy was examined in a lethal, noncompressible porcine liver injury model over 6 hours following injury. Wounds were packed with SMP foams, XStat, or QCCG and compared in terms of time to bleeding cessation, total blood loss, and animal survival. The hemostatic material properties and in vitro blood interactions were also characterized. SMP foams decreased blood loss and active bleeding time in comparison with XStat and QCCG. Most importantly, SMP foams increased the 6-hour survival rate by 50% and 37% (vs. XStat and QCCG, respectively) with significant increases in survival times. In parallel studies, modifications were made to the foams to make them degradable, which would allow for hemostatic materials to remain in place during healing, and antimicrobial to reduce infection risks.

CONTENTS

LIST OF FIGURES AND TABLES

LIST OF FIGURES AND TABLES

BODY MATTER

1. INTRODUCTION

Hemorrhage is the leading cause of potentially preventable death for soldiers on the battlefield and for civilians age 1-46 in the USA.[1,2] On the battlefield, standard hemorrhage treatment includes the use of tourniquets, pressure dressings, and impregnated (e.g. chitosan, kaolin) gauze, which may be insufficient for up to 80% of bleeding wounds, including non-compressible wounds in the torso.[3] Additionally, the use of tourniquets increases risk of nerve damage if applied for extended periods.[4] Up to 87% of bleeding deaths occur before reaching a fixed care facility;[5] thus, rapid bleed stabilization is essential for improving outcomes after major hemorrhagic injuries.

A current treatment option that is commonly used on the battlefield is QuikClot® Combat Gauze (QCCG), which contains a clay material called kaolin. Kaolin enhances blood coagulation at wound sites without inducing thermal damage.[6] While QCCG is effective in reducing blood loss, it has limited efficacy in improvised explosive device (IED) and small-caliber firearm wounds.[7–9] Another more recent hemostatic dressing on the market is XStat®. XStat is advised for use in narrow wounds, such as gunshots, and is part of the treatment algorithms in the Tactical Combat Casualty Care Guidelines. This system contains compressed, rapidly expanding chitosan-covered cellulose sponges. XStat improves hemostasis and ease of application with reduced mortality in animal models.[10] XStat is designed for filling in narrow wounds, rather than irregularly-shaped IED blast wounds, and it is only certified for use up to 4 hours to reduce ischemia risks.[11,12] This short application time limits XStat usage in the battlefield, as removal may not be possible within that time frame. IEDs were the leading cause of death in Iraq and Afghanistan between 2006 and 2018, accounting for 59% and 54% of hostile-related deaths, respectively, and there remains a need for an effective hemostatic dressing that can address IED wounds.[13]

To address this urgent clinical need, new gauze materials composed of fibrin and thrombin have been developed, with improvements in stable clot formation observed.[14] However, bovine- or porcine-based thrombin, a known coagulant, can induce an immune response.[15] Natural hemostatic polymer dressings have also been explored. For example, increasing porosity of traditional chitosan microspheres decreases clotting time by 133%.[16] However, hemostatic microparticle use increases embolism risks. Chitosan-coated diatoms were developed for use as a hemostatic dressing. The diatom, composed of porous silica, decreased clotting time when compared to clinical dressings.[17] Yet, diatoms can be difficult to synthesize

without contamination, reducing potential clinical applicability of this material.[18] Another materials-based approach to hemorrhage control includes injectable hemostatic systems. Using polyphosphate-conjugated hyaluronan, injectable hydrogels with quick gelation had similar blood loss with a decreased risk of embolism as compared to fibrin glues in a rat liver injury.[19] However, due to the high ambient temperatures of warzone climates, these hydrogel solutions could not be easily stored in liquid form, as they solidify into a gel-like substance at 37 °C. Alternate hydrogel systems have been synthesized to release batroxobin derived from snake venom. Batroxobin induces clotting even in the presence of heparin, but the cost of production limits its potential clinical use.[20]

A fully synthetic material system with the potential to overcome current treatment and research limitations is polyurethane shape memory polymer (SMP) foams. Thermo-responsive SMPs can be synthesized in a primary shape. Then, when heated above a thermal transition temperature, the SMPs can be deformed and stored into a low-profile secondary shape that is retained upon cooling. When a thermal stimulus is reapplied, the polymer reverts to the primary shape (**Figure 1**).[21] In a previous study by Wilson et al., highly crosslinked polyurethane foams were synthesized with ideal thermal properties for hemorrhage control.[22] Namely, this SMP foam system can be designed to have a high glass transition temperature (Tg) in dry conditions (45-80 °C) that is reduced to 15-45 ºC in aqueous environments (e.g. upon exposure to body temperature blood after implantation). Shape recovery can be tuned between 30 seconds to 30 minutes. Thus, SMP foams could be stably stored at high ambient temperatures in a first-aid kit and placed into a deep wound site in a compressed shape, where they would expand after exposure to water in body temperature blood to fit the irregular wound shape. These foams promote blood clotting due to the high surface area of the highly porous material and thrombogenic surface chemistry.[23] Stable clots were formed in porcine saccular aneurysm models, and in a porcine hind limb vessel, SMP foams induced arterial hemostasis within 90 seconds of device deployment.[23–26] Additionally, the polyurethane foams have proven biocompatibility in long-term animal implants over 180 days.[24]

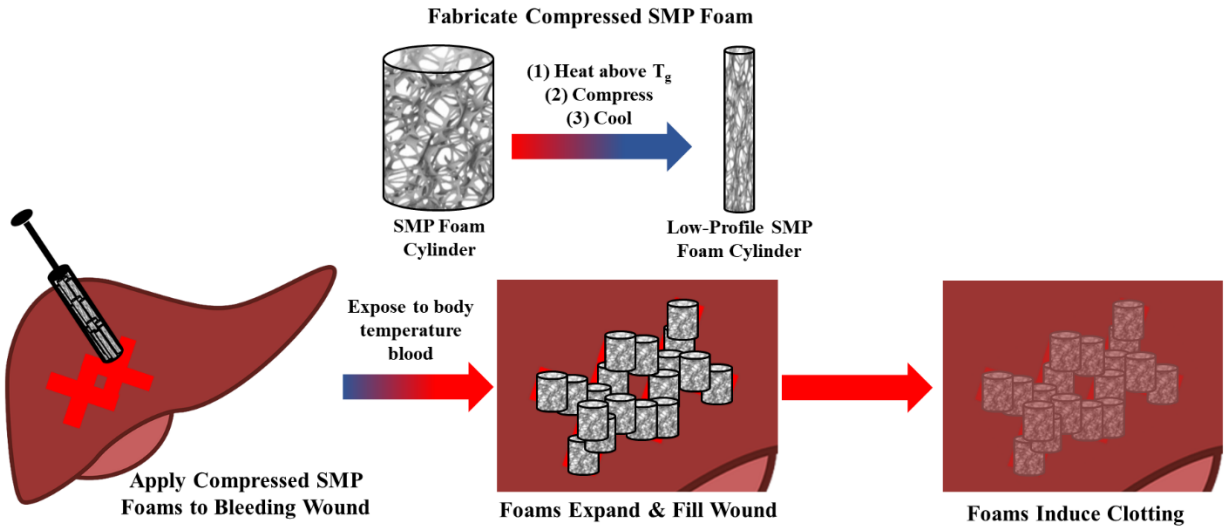

Figure 1. Schematic representation of the mechanism for SMP foams. Foams are heated above their glass transition temperature (Tg), then compressed into a low-profile secondary shape and stored. When the foams are inserted into the wound site and exposed to body temperature blood, they expand to the primary shape, filling the wound and causing clotting.

To build upon previous work that explores SMP foam usage in aneurysms and peripheral vascular disease, their efficacy was measured *in vivo* in a lethal hemorrhagic wound model. The liver is the most commonly injured abdominal organ causing hemorrhagic death; therefore, Pusateri et al. reported a model for inducing a Grade V liver injury in swine.[27] The wound is characterized by lethal amounts of parenchymal damage as well as vascular lacerations; Grade V vascular liver injury must lacerate at least two major blood vessels.[28] Using a similar model in this study, we examined the ability of SMP foams to stop bleeding within 30 minutes. We measured blood loss, active bleeding time, and animal survival for up to 6 hours after treatment with SMP foams in comparison with clinically available controls (XStat and QCCG). Then, to better understand results, material properties, *in vitro* blood interactions, and cytocompatibility were measured with the hemostatic materials.

2. EXPERIMENTAL SECTION

2.1 Foam Synthesis

Polyurethane foams were synthesized using the procedures described by Singhal et. al.[29] All monomers were purchased from Fisher Scientific (Waltham, MA). Briefly, this two-step process starts with an isocyanate (NCO) pre-polymer mix that contains 100 mol. eq. of isocyanate groups from hexamethylene diisocyanate (HDI) and 35 mol. eq. of hydroxyl (OH) groups, which come from triethanolamine (TEA) and N, N, N', N'-tetrakis(2-hydroxypropyl) ethylenediamine (HPED). The NCO pre-polymer mix was prepared inside a low-humidity glovebox (LabConco, Kansas City, MO) and reacted for 48 hours at 50ºC. A OH mixture was then prepared with the remainder of the OH monomers (TEA and HPED, 65 mol. eq. of OH groups), as well as foaming agents (catalysts, surfactants, and deionized (DI) water). Catalysts (T-131 and BL-22) and surfactants (EPH 1190) were provided by Evonik (Essen, Germany). DI water was used as a blowing agent to form CO_2 when reacted with isocyanates. The NCO and OH mixtures were combined and mixed using a high-speed mixer (FlackTek, Inc., Landrum, SC). The foams were then blown and cured at 50ºC for 5 to 10 min.

2.2 Foam Characterization

2.2.1 Pore Size: Foam slices (n = 3; 1 cm^2) were cut and sputter-coated with gold for 45 seconds, and then foam pores were imaged using Jeol NeoScope JCM-5000 Scanning Electron Microscope (SEM). Pore sizes were analyzed using a line drawn between the two farthest opposing pore walls on all complete pores visible within an image. Using ImageJ, diameters were measured and scaled to image size.

2.2.2 Density: Cubed samples from each foam (n = 7; 1 cm^3) were cut, and each wall dimension was measured using digital calipers to calculate volume. Foam pieces were weighed using a gravimetric scale. The density was calculated as mass per cubic centimeter.

2.2.3 Thermal Transitions: The glass transition temperature (Tg) of SMP foams (3-5 mg specimens) was measured using a Q-200 DSC (TA Instruments, Inc., New Castle, DE) under wet and dry conditions. Dry thermograms were obtained for each foam based on the following program: 1) temperature was decreased to 0 °C at 10 °C min^{-1} and held isothermally for 2 min; 2) temperature was increased to 80 °C at 10 °C min^{-1} and held isothermally for 2 min; 3) temperature was decreased to 0 °C at 10 °C min^{-1} and held

isothermally for 2 min; and 4) temperature was increased to 80 °C at 10 °C min^{-1}. The dry Tg was determined using the half-height of the inflection in the second heating cycle.

Prior to wet Tg measurement, foam samples were placed into a glass vial containing DI water. Vials were incubated at 50 ºC for 15 min to fully plasticize foams in water. The samples were removed from vials and patted dry using laboratory wipes. Wet thermograms were obtained for each foam based on the following program: 1) temperature was decreased to 0 ºC at 10 ºC min^{-1} and held isothermally for 2 min and 2) temperature was increased to 80 °C at 10 °C min^{-1}. The wet Tg was determined using the half-height of the inflection in the heating cycle.

2.2.4 Shape Recovery: Radially compressed foam cylinders (uncompressed diameter = 1.5 cm, length = 1.5 cm) were prepared using a BlockWise radial crimper (Tempe, AZ). Cylinders were heated to 70 ºC for 15 min and placed into the manual crimper to prepare compressed samples. Foams remained in the crimper for 5 min at room temperature to lock in the secondary compressed geometry. The diameters of the compressed foams were measured using digital calipers. Nickel titanium wire was threaded through the center of each sample and attached to a base plate in a 32 ºC water bath. Images were taken of the foam sample every 5 seconds for 5 minutes. The foam diameter was re-measured after 5 minutes using digital calipers. The images were analyzed using Insight Toolkit (ITK), where the foam area (number of pixels) was measured in each individual image and normalized using measurements acquired from the samples.

2.3 Foam Sample Preparation

Foam samples were in the form of compressed cylinders and powder. The cylinders (1.5 cm length) were prepared using a 1.5 cm diameter punch. For powder, horizontal sections of foam (~0.5 cm thick) were cut using a hot wire cutter. The sections were then cut into 8 cm X 11 cm sheets. Cylinders and sheets were cleaned using a 10X volume wash of 70% ethanol and 20X volume wash of DI water. Each wash was preformed twice on a shaker table for 5 min at 100 rpm. Samples were then dried under vacuum at room temperature for 24 hours and radially crimped as described in shape recovery testing. Powders were made from non-programmed sheets via blending in a standard kitchen blender until only fine powder pieces remained.

2.4 In Vivo *Hemorrhagic Injury Model*

All procedures were approved by the State University of New York (SUNY) Upstate Medical University Institutional Animal Care and Use Committee (IACUC #453 Rev.). Female Yorkshire swine (35-45 kg) were purchased from a certified dealer and acclimated at the SUNY Upstate Medical University facility for 1 week. A total of 24 pigs were tested in this study. Each hemostatic dressing type (XStat, QCCG, and SMP foam) was tested on 8 pigs. On the day of the procedure, animals were anesthetized using atropine (0.54 mg/mL, intramuscular) and telazol (5 mg/kg, intramuscular). Anesthesia was maintained intravenously using ketamine (90 mg/kg) and xylazine (10 mg/kg) at a rate of 1 mg/kg/hr. A surgical plane of anesthesia (Gudel's classification Plane III) was maintained at all times. Baseline blood samples were taken to assess platelet count, prothrombin time (PT), and hemoglobin. Ice cold Ringer's solution was administered intravenously to dilute the animal blood and reduce body temperature until the hematocrit was reduced by a minimum of 25%. Ice was placed inside the abdomen of the animal simultaneously with the administration of Ringer's solution to aid in reducing the core body temperature to 31.5 ± 1.5 ºC.

A Grade V liver injury was then induced using the tool shown in **Figure 2B**. The blades were inserted between the left and right medial lobes of the liver, then the tool was dragged slightly laterally. The tool was retracted, overlapped with the previous insertion by ~50%, and dragged slightly in the opposite direction to provide a wound like that shown in **Figure 2A**. The wound was allowed to freely bleed for 30 seconds, and then the hemostatic intervention was applied. Suction was applied to remove lost blood during trials. XStat and QCCG were manually applied to the wound. SMP foam cylinders were applied manually to fill the major spaces, and then powder was applied from a modified (open) syringe to fill in smaller crevices. Manual pressure was applied for 60 seconds and then briefly removed to check if the bleeding had ceased. This step was repeated until the bleeding was stabilized or for up to 30 minutes. Trial time was stopped when bleeding ceased. If the wound failed to cease bleeding within the allotted time, then all interventions were stopped. If bleeding ceased, the total blood loss was measured from the suctioned blood container, and the animal was evaluated for up to 6 hours while under anesthesia. The animal was then euthanized via an injection of sodium pentobarbital. Upon completion of the trial, the amount of each material used was determined as follows:

$$SMP\ foam\ amount = \left(Cyl_{Used} \times Cyl_{Avg\ mass}\right) + \left(Powder_{Orig} - Powder_{Final}\right)$$

$$XStat\ amount = Cyl_{Used} \times Cyl_{Avg\ mass}$$

$$QCCG\ amount = Packs_{Used} \times Pack_{Avg\ mass}$$

Where Cyl_{Used} is the number of SMP foam or XStat cylinders applied to the wounds; $Cyl_{Avg\ mass}$ is the average mass of SMP foam or XStat cylinders, respectively; $Powder_{Orig}$ is the amount of pre-weighed powder added to the open syringe before the study began; $Powder_{Final}$ is the amount of powder left in the syringe after the study was complete; $Packs_{Used}$ is the number of QCCG packages applied to the wounds; and $Packs_{Avg\ mass}$ is the average mass of a QCCG package.

Histogical samples were taken from the wound site and placed in formalin (QCCG: n=8, SMP: n=7, XStat: n=6) . The samples were then sent HistoWiz, Inc (Brooklyn, NY), where they were stained with haematoxylin and eosin. Two independent assessments were made on resulting images to characterize hepatocellular and vascular damage, hemostatic action, and any reparative processes.

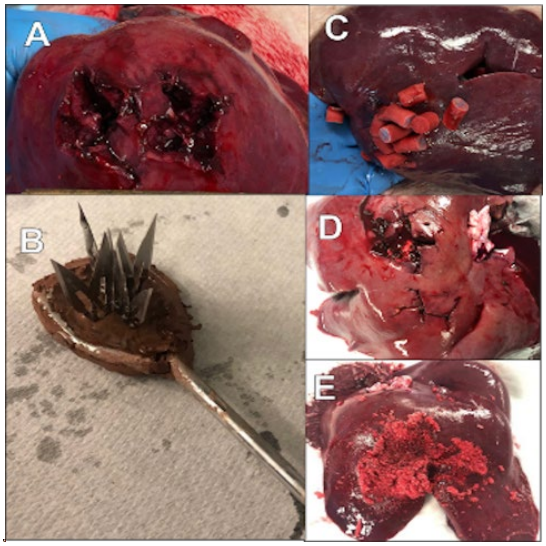

Figure 2. (A) Image of wound after inducing grade V liver injury. Wound was created using cutting tool (B). Images of liver after treatment with (C) XStat, (D) QCCG, and (E) SMP foams.

2.5 Hemostatic Dressing Characterization

2.5.1 Water and Blood Absorption: All tested hemostatic dressings (XStat, QCCG, and SMP foams) were weighed to determine dry weight (W_d). The dry dressings were placed into either a water bath for 1, 5, 10, and 30 minutes at 32 ºC or into whole blood for 5 and 30 minutes at 37 ºC. Whole porcine blood was

purchased from Lampire Biological Laboratories (Pipersville, PA). Blood was anticoagulated with Na-Citrate upon collection stored at 4°C for up to 3 weeks from the bleed date, according to supplier guidelines. When removed from water or blood, samples were lightly patted dry to remove excess surface liquid. The dressings were then weighed to obtain the wet weight (W_w). Fluid absorbtion was calculated as:

$$Fluid\ Absorption = \frac{W_w - W_d}{W_d} \times 100\%$$

Where W_w is the weight of the sample in water or blood, and W_d is the dry mass.

2.5.2 Compressive Mechanical Properties: Cylindrical samples, approximately 2:1 diameter to height ratio, were acquired from each of the hemostatic materials (XStat, QCCG, and SMP foams), and compressive mechanical properties were measured in dry and wet conditions. Since QCCG is a single sheet, pieces were stacked until the desired height was obtained. Wet samples were placed into a 32 ºC water bath for 10 minutes prior to testing. All samples were compressed at a rate of 5 mm min^{-1}. Testing was automatically stopped at a load reading of 24 N. Stress and strain were then calculated from the collected data. Modulus was obtained from the slope of a linear regression of all data points between 2 and 10 % strain.

2.5.3 Hemolysis: Samples (n=6) were cut into pieces with surface areas of approximately 145 cm^2. Before the experiment, samples were incubated in 1X PBS for 5 hours. DI water (hemolytic) and PBS (non-hemolytic) served as controls. Samples were transferred to a 15 ml centrifuge tube containing 5 mL of fresh PBS warmed to 37 ºC. Anticoagulated porcine blood was heated at 37 ºC for 15 minutes prior to use. Then, 100 µL of blood was added to each sample and controls, and tubes were incubated in a 37°C water bath for 1 hour. The sample tubes were centrifuged at 1000 rpm for 10 minutes. The supernatant (200 µL) was added to a 96-well plate and a microplate reader was used to measure optical density (OD) at 545 nm, the absorbance of released hemoglobin. Hemolysis was calculated by:

$$Hemolysis\ (\%) = \frac{OD_{sample} - OD_{PBS}}{OD_{DI\ water} - OD_{PBS}}$$

2.5.4 Platelet Attachment and Activation: Samples were cut into thin slices (0.5 cm^3) and placed into a 24 well-plate with 1 ml of anticoagulated whole blood at 37ºC for 30 minutes. Samples were then rinsed with 1X phosphate buffered saline (PBS) to remove non-attached platelets and fixed in 2% glutaraldehyde at 4ºC overnight. The fixed samples were dehydrated in a series of ethanol solutions (50%,

70%, 95%, and 100%) for 30 minutes each. Upon completion of the dehydration, samples were dried overnight in a room temperature vacuum oven. The samples were then sputter-coated with 5-10 nm of gold and imaged using a SEM at 15 kV. Images obtained were qualitatively analyzed for platelet aggregation and morphology changes.

2.5.5 Coagulation Time: Samples (n=4) were cut and placed in 1.5 ml tubes to analyze relative clotting time over 30 minutes. Empty tubes served as negative controls. Prior to testing, blood was heated to 37 ºC, and then 1M $CaCl_2$ solution was added to the blood to attain a 0.01M $CaCl_2$ concentration to reverse the anticoagulant. Immediately after reversing the anticoagulant, 50 µL of blood was added to each sample. At each time point over up to 30 minutes, 1 ml of DI water was added to stop the clotting process and lyse-free red blood cells. The samples were centrifuged at 2300 rpm for 15 minutes, and then 200 µL of lysates were placed into a 96 well-plate. Using a microplate reader, absorbances were obtained at 540 nm.

2.5.6 Cytocompatibility: NIH/ 3T3 mouse fibroblasts were cultured in Dulbecco's Modified Eagle Medium supplemented with 10% fetal bovine serum and 1% penicillin-streptomycin. All testing was completed at least one passage after thawing from liquid nitrogen. Cells were seeded at 10,000 cells per well in a 24 well plate. XStat and SMP pieces were placed into 70% ethanol overnight then placed into sterile phosphate buffer solution for 1 hour prior to testing. QCCG was used directly from the sterile packing. Samples were placed into Transwell inserts in wells above pre-seeded cells. After 24 hours, inserts containing samples were removed. Fresh media containing a 10% resazurin dye (Alamarblue™) was added to the cells and allowed to incubate for 2 hours. Florescence was measure in each well (excitation 530 nm and emission 590 nm). Each testing group was compared to an untreated control. Cytocompatibility was calculated by:

$$\text{Cell Viability (x)} = \frac{Abs(Hemostat)}{Abs_{Control}} \times 100\%$$

Where the control is cells incubated with empty inserts.

2.6 Data analysis

A power analysis was carried out based upon our pilot model data using Microsoft Excel (template provided by Boston University's IACUC; 80% power, α = 0.05) to determine the sample size of 8 pigs. Data collected before the injury (**Table 1**) was examined by a single factor ANOVA within Excel with an alpha

value of 0.05. All other data were analyzed by a two-tailed equal variance Student's T-test within Excel comparing XStat, QCCG, and SMP foams. A p-value less than 0.05 was considered statistically significant.

3. RESULTS AND DISCUSSION

3.1 Foam Characterization

Initial foam characterizations are summarized in Table 1. Foam Tg was 53 ± 2 ºC and 25 ± 3 ºC in the dry and wet conditions, respectively. As these SMPs would be used in combat applications, they must maintain their compressed state at high ambient temperatures; thus, the high dry Tg provides an initial indication of this capability. Future work will focus on preparing a storage and delivery device that enables stable storage and facile delivery of compressed foams. The low wet Tg allows actuation once in contact with blood at 37 ºC (or lower, in the case of reduced body temperature induced by shock) Lower wet Tg is due to water plasticization, where water disrupts hydrogen bonds between polymer chains to increase flexibility. The mean pore size was 867 ± 59 μm, and the foam density was 0.04 ± 0.01 g cm $^{-3}$. The low density and large pores size aid in compression and expansion of SMP foams and in increasing surface area for clotting. The volume at 0 hours post-crimping refers to the volume to which the polymers were radially crimped into a constricted shape, which was 22% relative to the original volume in the expanded state. After crimping, foams were stored in dry conditions for 24 hours, and volumes were measured again to provide an indication of shape fixity over 24 hours at room temperature. The polymers did expand slightly during storage to ~29% of the original volume, but overall, they maintained their temporary, crimped geometry.

Table 1. SMP foam properties. Tg was measured under wet and dry conditions using DSC. Pore sizes were imaged using SEM and quantified with ImageJ. Volumes and masses of small foam sections were measured for density. Radially compressed cylinders were measured directly after crimping and then stored at room temperature for 24 hours and measured. n = 7; Mean ± 95% confidence interval displayed.

Property	**Measurement**
Dry Tg	53 ± 2 ºC
Wet Tg	25 ± 3 ºC
Pore Size	867 ± 59 μm
Density	0.04 ± 0.01 g cm^{-3}
Volume at 0 Hours Post-Crimping	22 ± 1%
Volume at 24 Hours Post-Crimping	29 ± 7%

3.2 Baseline Blood Data

Based on the results presented in **Table 2**, all *in vivo* experimental groups were comparable prior to treatment. There were no significant differences in percent change in hematocrit prior to injury and treatment. The mean amount of Ringer's solution required to achieve a minimum of 25% hematocrit

reduction was 3225 ± 383, 3881 ± 579, and 3225 ± 659 ml with respect to pigs treated with XStat, QCCG, and SMP foams, with no significant differences between the groups. Mean arterial pressure (MAP) between the tested animals was between 110 and 120 mmHg with no significant difference between testing groups. Baseline blood analysis showed no significant difference between the groups in all categories except fibrinogen, which was slightly lower in the XStat group.

Table 2. Summary of baseline blood data and 30 second uncontrolled blood loss amount for each treatment group. Mean ± 95 % confidence interval displayed.

	XStat	QCCG	SMP Foam	p Value
Number of animals	8	8	8	
Animal weight (kg)	41.1 ± 1.5	39.2 ± 1.2	40.8 ± 1.7	0.182
Baseline MAP (mmHg)	101 ± 17	119 ± 11	119 ± 9	0.136
Hematocrit decrease (%)	33.0 ± 3.3	30.2 ± 4.4	31.7 ± 4.7	0.652
Hemoglobin (g/dl)	9.7 ± 0.6	9.9 ± 0.6	9.5 ± 0.5	0.579
Platelets (1,000/ mm^2)	260 ± 86	333 ± 47	306 ± 65	0.348
Prothrombin time (s)	14.3 ± 0.3	13.9 ± 0.2	14.1 ± 0.3	0.163
Fibrinogen (mg/dL)	172 ± 16	206 ± 17	209 ± 26	0.040
Ringer's solution (ml)	3225 ± 383	3881 ± 579	3225 ± 659	0.189
30 sec. blood loss (ml)	483 ± 92	442 ± 150	381 ±107	0.549

3.3 Active Bleeding Time and Blood Loss

XStat (n=8) had the longest mean active bleeding time (28.9 ± 2.1 min), **Figure 3a**. QCCG (n=8) performed 8% better than XStat (26.7 ± 4.25 min). SMP foam (n = 8) treatment significantly decreased active bleeding time (20.6 ± 6.9 min) in comparison to XStat ($p = 0.04$) and resulted in 28% and 23% decreased active bleeding time compared to XStat and QCCG, respectively. Mean blood loss was highest in pigs treated with XStat and QCCG (1287 ± 323 and 1287 ± 385 ml, respectively). Mean blood loss after treatment with SMP foams was 11.2% lower than with other treatments, with a loss of 1142 ± 316 mL, **Figure 3b**.

It is important to note that the XStat applicator was not used in this study. During the pilot studies, it was found that it provided more control over placement to insert XStat samples by hand in the wounds. It is possible that using the applicator could have improved XStat's performance. It should also be noted that XStat is indicated for use in compressible, narrow tunneling wounds rather than the irregularly shaped liver wounds in these studies, which may have affected its relative efficacy. SMP foam cylinders

were added by hand, and powdered SMP material was applied separately using a syringe with the nozzle tip removed to enable containment of powder. We hypothesize that the SMP foam powder increased the exposed surface area of the hemostatic material and allowed for increased blood trapping and coagulation in wound crevices to reduce active bleeding time. In future studies, improvements to the SMP foam application system could be made to further decrease active bleeding time.

While blood losses were not significantly different between the treatment groups, SMP foams on average had reduced bleeding times and corollary reduced blood loss. In a previous study, QCCG combat gauze treatment resulted in a blood loss of 1397 ± 806 ml.[27] The observed blood loss with QCCG in the current study was comparable (1287 ± 556 ml). The previous study did not consider temperature changes due to blood loss or set a maximum time frame for the testing trial. In the current model, the pig body temperature was decreased to simulate shock and further reduce clotting capabilities, and resuscitation efforts were abandoned after 30 minutes.[29] Similar hemorrhage volumes were also observed when testing using a blood substitute in an *in vitro* grade V liver injury model, in which no significant differences were observed between XStat, QCCG, and SMP foams.[30]

3.4 Survival

With the use of powder foams, there is an increased risk of embolism.[16] Thus, after the initial 30 minute trails, pigs were observed under anesthesia for 6 hours before determining survival. Several previous studies using a similar model included a 1 hour watch period.[27,31] However, on the battlefield, a patient may not be able to receive care at a fixed facility with surgical capabilities for several hours.[32] XStat caused a significant amount of visible parenchymal damage with increased packing during treatment. Removal of packed XStat was required to re-administer the dressing and prevent wound tearing in the non-compressible wounds. QCCG also had to be removed to repacked, but the gauze-like material made removal much easier in comparison to the smaller pieces of XStat. XStat and QCCG treatment 30-minute survival rates were 12.5% and 25% (1/8 and 2/8 pigs), respectively, **Figure 3c**. Of the two pigs treated with QCCG that achieved bleeding cessation within the trial time of 30 minutes, one survived the full 6-hour watch period. While performing interventions with QCCG, bleeding would slow, but as MAP increased, clots would fail, leading to a continuation of bleeding at the wound site.

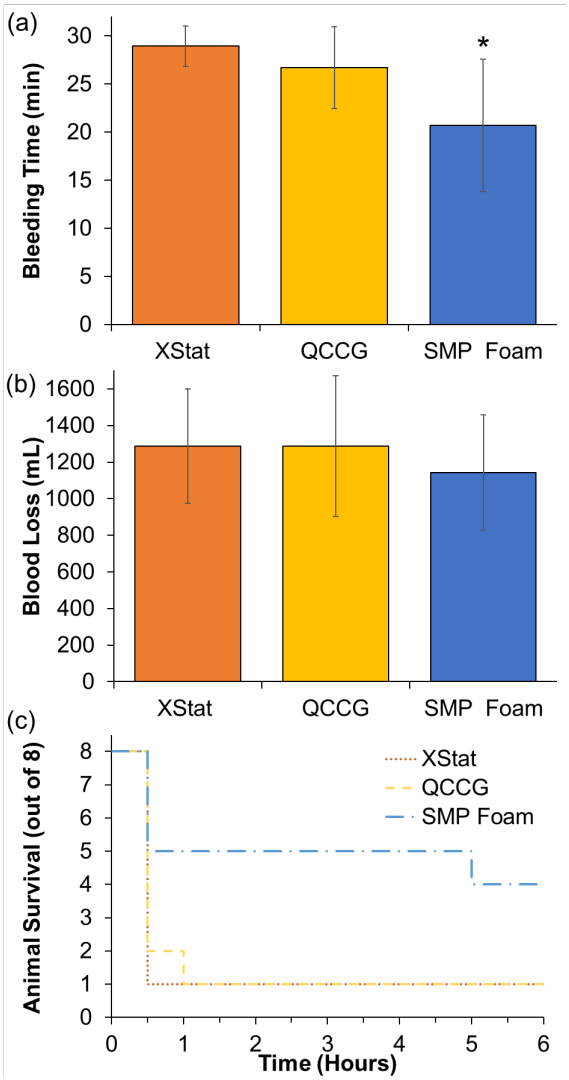

Figure 3. Grade V liver injury (a) active bleeding time and (b) blood loss after treatment with XStat, QCCG, and SMP foams. Mean ± 95 % confidence interval displayed, n=8. *p<0.05 relative to SMP foam (p-values: XStat vs. SMP foam bleeding time: 0.04; QCCG vs. SMP foam bleeding time: 0.11; XStat vs. SMP foam blood loss: 0.36; QCCG vs. SMP foam blood loss: 0.35) (c) Animal survival over 6 hours post-grade V liver injury after treatment with hemostatic dressings, n = 8. (p-values of animal survival times: XStat vs. SMP foam: 0.04; QCCG vs. SMP foam: 0.05).

SMP foam treatment resulted in the highest 30-minute survival with 5/8 (62.5%) surviving animals. Of the five pigs that achieve hemostasis after treatment with SMP foams, four survived the full six-hour duration. The fifth pig died due to possible fluid overload after the fifth hour, causing cardiac failure. SMP foam treatment significantly increased average survival times over the 6-hour study (3.8 ± 1.0 hr for SMP foams vs. 1.3 ± 0.7 hr for QCCG (p = 0.05) and 1.2 ± 0.7 hr for XStat (p = 0.04)).

3.5 Histological Analysis

Table 3. Summary of the visual histological analysis from pigs treated with XStat (n=6), QCCG (n=8), and SMP (n=7). The evaluation period separates animals that survived 0.5-1 hour from those that survived 5-6 hour. No statistically significant differences were observed between treatment groups or evaluation periods (all p>0.05).

Sample	**XStat**		**QCCG**		**SMP**	
Evaluation period	0.5-1 hr n=5	5-6 hr n=1	0.5-1 hr n=7	5-6 hr n=1	0.5-1 hr n=2	5-6 hr n=5
Hepatocyte degeneration/ necrosis	2/5	0/1	1/7	1/1	1/2	2/5
Hepatocyte degeneration/ necrosis depth (mm)	0.3 ± 0.4	--	0.1 ± 0.4	2.5	0.5 ± 0.7	1.4 ± 2.2
Loss of hepatic architecture	5/5	1/1	6/7	1/1	1/2	5/5
Loss of hepatic architecture depth (mm)	1.0 ± 0.4	1	1.3 ± 1.1	2.5	0.5 ± 0.7	2.6 ± 1.4
Interstitial edema	0/5	0/1	0/7	0/1	0/2	1/5
Vascular microthrombi	0/5	0/1	0/7	0/1	0/2	1/5
Inflammation	2/5	0/1	2/7	0/1	0/2	2/5
Inflammation depth (mm)	0.5 ± 0.9	--	0.2 ± 0.4	--	--	1.1 ± 2.2

Overall, there were very few observable histological differences between treatment groups or between animals that survived the full 6 hours in comparison with those that died in the first hour, **Table 3** and **Figure 4** (no statistically significant differences ($p < 0.05$) for any measurement). Hepatocyte necrosis was observed in all treatment groups at depths that ranged from 0 to 5 mm. Loss of hepatocyte architecture was highest in XStat (100% of animals), but all but two animals (1 treated with QCCG and 1 treated with SMP foam) in the study had a loss of hepatocyte architecture. The observed necrosis and loss of hepatocyte architecture are attributed to the injury formation and not the hemostatic materials. After XStat and QCCG treatment, more inflammation was observed in the 0.5-1 hour survival group (2 animals each) than in the 5-6 hour survival group. Inflammation was higher in the 5-6 hour survival group with SMP foams (2 animals) in comparison with the SMP foam 0.5-1 hour group. Overall, the number of apparencies (n=2) was the same for all testing groups; thus, differences in inflammation are again likely due to the injury itself, rather than material properties. One instance of vascular microthrombi was observed after SMP foam treatment. This result may be due to the use of the SMP foam powder, as these pieces could be small enough to enter the vasculature. However, the only occurrence of microthrombi was observed in an animal that survived the entire 6-hour watch period. Therefore, while there is the potential formation of microthrombi, the microthrombi did not cause fatal embolism in the animal. In future studies, histology will be completed on

downstream organs (e.g., gut and kidneys) to confirm that the foams remain in the wound site and that there are no adverse ischemic events after SMP foam treatment.

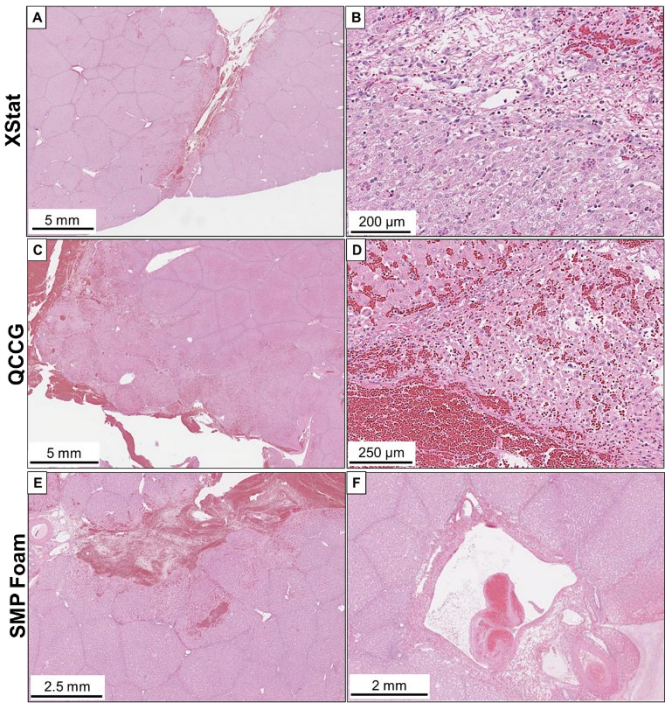

Figure 4. Hematoxylin and eosin staining of porcine liver sections: A-B) from a pig treated with XStat that died by 0.5 hour. A) Zone of architectural disruption with congestion and hemorrhage surrounding the site of injury. Around this zone, the hepatic parenchyma appears unremarkable. B) Transition from the area of disruption, hemorrhage, and degeneration of hepatocytes (top of the image) to the less affected tissue (bottom of the image). C-D) From a pig treated with QCCG that survived 6 hours. C) Immediately above the area of injury, there is a zone of architectural distortion with congestion and hemorrhage. Above this zone, an area of less affected hepatic tissue is noted. D) Higher-power view with evidence of disruption of hepatic plates, congestion of sinusoids, hemorrhage, and degeneration/necrosis of hepatocytes. E-F) From a pig treated with SMP Foam that survived 6 hours. A) Zone of architectural disruption with congestion and hemorrhage surrounding the site of injury. Below this zone, the hepatic parenchyma is well preserved. B) Non-occlusive microthrombus observed in a vessel close to the area of injury.

3.6 Hemostatic Dressing Material Properties

Table 4. Hemostatic material density, material used in implantation, and compressive modulus values in the wet and dry state. Mean ± 95 % confidence interval displayed. A p-value <0.05 indicates a significant difference compared to SMP foams.

Sample	Density (g/cm^3)	Material Used (g)	Estimated Volume Used (cm^3)	Compressive Modulus (kPa)	
				Dry	Wet
XStat	0.05 ± 0.01 p = 0.07	5 ± 1 p = 0.004	~96	170 ± 26 p = 0.4	8.9 ± 1.5 p = 0.02
QCCG	0.02 ± 0.01 p =0.000004	34 ± 7 p = 0.002	~1700	25 ± 16 p = 0.0008	7.2 ± 5.6 p = 0.612
SMP Foam	0.04 ± 0.01	15 ± 6	~370	211 ± 88	3.8 ± 2.0

Since SMP foams lack any procoagulant drugs, their previously observed increased clotting is attributed to the high surface area and thrombogenic, hydrophobic material chemistry.[33] The large interconnected pores allow for a high influx and trapping of blood into the foams.[34] In the current study, the porous powder pieces likely further aided blood interactions with the embolic surface and subsequent clotting. To better understand the clotting mechanisms of the three materials, they were characterized *in vitro*.

All hemostatic materials have very low density, which is attributed to their porous and/or fibrous structures. When the densities are taken into consideration with the amount of material used in the liver injury model, the estimated volume used of QCCG is much higher than that of XStat (lowest estimated volume) and SMP foams, **Table 4**. To further explore potential implantation forces that may have affected hemostatic material efficacy, modulus was measured in the dry and wet states. The dry modulus provides some information on the ability to work with the materials before implantation and aqueous environment exposure. The wet modulus measurements enable analysis of the potential effects of the materials on wound wall pressures after implantation. Mechanical compression testing (**Table 4**) showed that all three materials are less stiff after water exposure. Both XStat and the SMP foams show significant changes in modulus when wet, which is attributed to water induced plasticization. In the wet state, SMP foams had the lowest compressive modulus (3.8 ± 2.0 kPa), which correlates with qualitatively reduced wound tearing observed during packing. While wet QCCG had a statistically comparable modulus to SMP foam (7.2 ± 5.6 kPa), its stiffness is much more variable, and over 4.5X more QCCG material was required for treating injuries in comparison to SMP foam volume (**Table 4**). The increased amount of material needed for wound packing would therefore induce higher wall pressures.

When comparing XStat and SMP foam wet modulus values and volume required for testing, there is not a clear correlation between these properties and the improved survival observed after SMP foam treatment. Thus, we hypothesize that expansion rates also played a factor in hemostatic material effectiveness. XStat shows much faster expansion rates in comparison to SMP foams, **Figure 5 a-b**. Fast actuation of XStat could lead to higher initial wound wall pressure, causing potential tissue tearing. Another consideration is the swelling profiles of the materials, **Figure 5c-d**. XStat quickly uptakes a large amount of water and reaches equilibrium water absorption. This property may account for minimal differences in

measured blood loss in the porcine liver injury, despite increased bleeding times after XStat treatment. SMP foam powder and cylinders absorb less overall water in comparison to XStat, with comparable water absorption to QCCG, **Figure 5c**. SMP foam cylinders are slower to research absorption equilibrium (~5 minutes) in comparison with SMP foam powder, XStat, and QCCG (~1 minute). It should also be noted that none of the hemostatic materials undergo large volume changes in the wet state, **Figure 5d**.

In general, there is likely a balance between the need for quick shape recovery to effectively fill irregularly shaped traumatic wounds without being expelled by high blood flow pressures; low modulus and correspondingly low wall pressures to prevent wound tearing; and blood absorption and interactions. Actuation rates and modulus could be tuned in SMP foams by altering pore size and/or interconnectivity, which would also affect blood permeability.[25,35,36] Our previously developed *in vitro* liver injury model will serve as a valuable platform in future work to further explore the roles of these properties in hemorrhage control.[30]

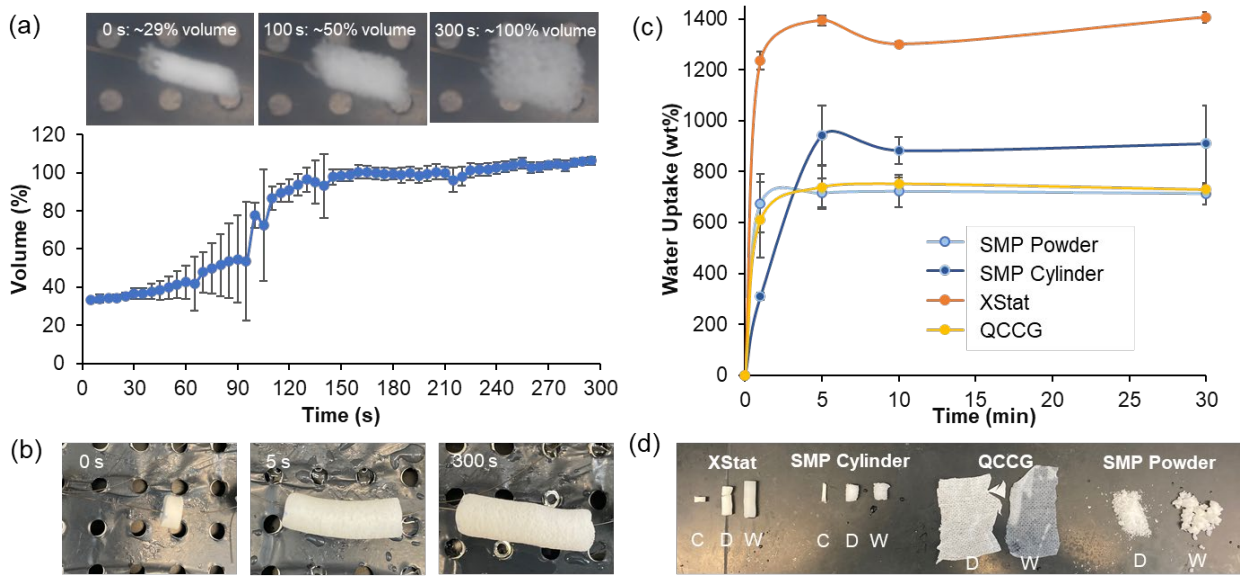

Figure 5. Hemostatic material interactions with water. (a) Volume recovery profile of SMP foam cylinders in water at 32°C. (b) Images of XStat after being placed into water at 32°C for 0, 5, and 300 seconds. (c) Water absorption profiles of all tested hemostatic materials over 30 minutes. (d) Images of XStat and SMP foam cylinders in their compressed, dry, and wet state and of QCCG and SMP foam powders in the dry and wet state. Wet state images were taken after 24 hours in water at 32°C.

3.7 In Vitro *Blood and Cell Interactions with Hemostatic Dressings*

Table 5. Hemostatic material biological properties: blood absorption, hemolysis, and cytocompatibility. Mean ± 95 % confidence interval displayed. Blood absorption p-values represent the comparison between 30 and 5 minute measurements for each material. Hemolysis p-values represent comparisons with SMP foams.

Sample	Blood Absorption (%)		Hemolysis (%)	Cytocompatibility at 24 Hours (%)
	5 min	30 min		
XStat	1407 ± 231	1455 ±115 p = 0.52	15.5 ± 25.8 p = 0.19	91 ± 7
QCCG	1692 ± 172	2009 ± 276 p = 0.28	0.0 ± 0.2 p = 0.41	96 ± 4
SMP Foam Cylinder	563 ± 29	570 ± 65 p = 0.87	0.0 ± 0.2	100 ± 11
SMP Foam Powder	994 ±179	1065 ±129 p = 0.61	--	96 ± 3

To better understand the role of blood/material interactions in the liver injury study, the hemostatic materials were characterized *in vitro* in terms of blood absorption, hemolysis, platelet interactions, and cytocompatibility. The largest blood absorption was seen in QCCG at both 5 and 30 minutes. XStat had comparable blood absorption to QCCG at 5 minutes (p= 0.22), but had significantly lower absorption at 30 minutes (p = 0.032). This result is the opposite of that observed in the water absorption profiles, where XStat had the highest water absorption and QCCG had the lowest. We attributed these trends to the presence of non-chemically attached clotting agents in QCCG that increases its blood interactions relative to its water interactions. SMP foam cylinders had the lowest amount of absorbed blood at both 5 and 30 minutes. Beyond the addition of clotting agents in QCCG, we attribute these trends to the pore sizes of the materials. XStat and QCCG both have more closed networks, qualitatively based on SEM images taken of tested materials, which may increase the amount of trapped blood when moving materials from the fluid to the scale in comparison with SMP foam cylinders. SMP foam powders showed higher blood absorption than cylinders, which was again opposite from the observed water absorption trends. The foam powder can spread out from each other in blood, which may increase the size of clots between individual pieces to increase overall blood absorption.

The highest hemolysis occurred in XStat, with high variability in measurements (15.5 ± 25.8, **Table 5**). QCCG and SMP foams induced no significant hemolysis (0.0 ± 0.2% for both samples). We confirmed that all materials have high cytocompatibility (>90%) with 3T3 fibroblasts, **Table 5**, indicating that any potential hemolytic properties of XStat do not negatively affect surrounding cells. However, it is possible that hemolysis induced by XStat may have contributed to some of the animal deaths in the *in vivo* study. To better understand clotting mechanisms, platelet interactions and coagulation times were measured with the three materials.

To analyze platelet interactions, SEM images were taken of material surfaces after incubation in whole blood that contained an anticoagulant, **Figure 6a**. These images revealed that XStat had remarkably limited levels of platelet attachment, with highly rounded platelets, indicative of no activation. Based on this result, we hypothesize that XStat may not be as effective at promoting clotting in the presence of an anticoagulant. The QCCG samples contained areas of aggregated and activated platelets with thrombus formation. The SMP foam had less mature platelet aggregates in comparison with QCCG, but there was a high density of platelet attachment and activation, evidenced by protrusions on platelet surfaces.

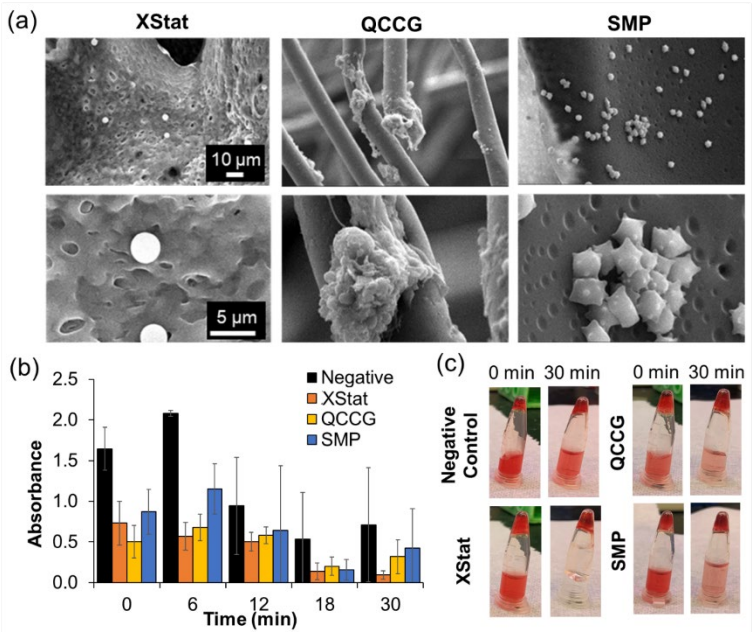

Figure 6. Summary of *in vitro* blood interactions. (a) Platelet interaction visualized via SEM images obtained at magnifications of 1000x (top row) and 5000x (bottom row). (b) Coagulation times were examined by hemoglobin release assay with (c) visual images of representative samples at 0 and 30-minute time points.

There were no significant differences in coagulation levels in blood with reversed anticoagulant, **Figure 6b** and **c**, but all samples showed improvements when compared to the empty tube control at the 0-minute mark, indicating that all three materials promote comparable and rapid coagulation in whole blood. This result generally corresponds with the comparable coagulation times and blood loss levels in the *in vivo* model.

Taken together, the *in vitro* and *in vivo* material characterization and blood interaction data indicates that XStat may have a hemolytic effect, which could have contributed to mortality after treatment. Also, XStat may be less effective in a patient that is taking anticoagulants, since there were minimal platelet interactions with the anticoagulated whole blood. QCCG showed evidence of increased clotting capabilities relative to SMP foams *in vitro* based on the platelet interactions. There are more complex processes at play in an actively bleeding non-compressible wound, which could be explored further in future work in an *in vitro* injury model with whole blood. We hypothesize that the combination of less stiff mechanical properties and low density of SMP foams in the wet state along with their ability to fill in complex wound geometries during controlled shape recovery contributed to the improved survival in the porcine model. These factors are important considerations for designing hemostatic materials for noncompressible bleeds. In addition to the benefits shown in the *in vivo* study, SMP foams have an advantage in their high level of chemical tunability. In future work, the foams could be modified with functional groups that increase coagulation, reduce infection risks, and/or provide localized pain relief. Overall, SMP foams provide a promising platform for hemorrhage control in noncompressible wounds.

4. CONCLUSIONS

These studies indicate that SMP foams have potential for improved efficacy in hemorrhage control in comparison to QCCG and XStat in a Grade V liver injury. SMP foam treatment resulted in decreases in bleed stabilization time and improved animal survival. The *in vitro* characterizations indicate the material properties (e.g., stiffness and shape memory capabilities) played a role in the improved *in vivo* outcomes. Based on the results of this study, the SMP foam system shows benefits for use as a hemostatic material in lethal, non-compressive hemorrhages in comparison with clinically available treatments. Future work will focus on longer term acute (24 hours) and subacute (up to 27 days) toxicity, sensitization, and irritation testing to ensure biocompatibility of SMP foams for hemorrhage control.

Notes

Research was conducted in compliance with the Animal Welfare Act, the implementing Animal Welfare regulations, and the principles of the Guide for the Care and Use of Laboratory Animals, National Research Council. The facility's Institutional Animal Care and Use Committee approved all research conducted in this study. The facility where this research was conducted is fully accredited by the AAALAC.

REFERENCES CITED

1. Eastridge BJ, Hardin M, Cantrell J, et al. Died of wounds on the battlefield: causation and implications for improving combat casualty care. *J Trauma*. 2011;71(1 Suppl):S4-8. doi:10.1097/TA.0b013e318221147b
2. Chambers JA, Seastedt K, Krell R, Caterson E, Levy M, Turner N. “Stop the Bleed”: A U.S. military installation’s model for implementation of a rapid hemorrhage control program. *Mil Med*. 2019;184(3-4):67-71. doi:10.1093/milmed/usy185
3. Walters TJ, Mabry RL. Issues related to the use of tourniquets on the battlefield. *Mil Med*. 2005;170(9):770-775.
4. Nitz AJ, Matulionis DH. Ultrastructural changes in rat peripheral nerve following pneumatic tourniquet compression. *J Neurosurg*. 1982;57(5):660-666. doi:10.3171/jns.1982.57.5.0660
5. Eastridge BJ, Mabry RL, Seguin P, et al. Death on the battlefield (2001–2011). *J Trauma Acute Care Surg*. 2012;73(6 SUPPL. 5):S431-S437. doi:10.1097/TA.0b013e3182755dcc
6. Sairaku A, Nakano Y, Oda N, et al. Rapid hemostasis at the femoral venous access site using a novel hemostatic pad containing kaolin after atrial fibrillation ablation. *J Interv Card Electrophysiol*. 2011;31(2):157-164. doi:10.1007/s10840-011-9552-6
7. Devlin JJ, Kircher S, Kozen BG, Littlejohn LF, Johnson AS. Comparison of ChitoFlex®, CELOX™, and QuikClot® in control of hemorrhage. *J Emerg Med*. 2011;41(3):237-245. doi:10.1016/j.jemermed.2009.02.017
8. Schauer SG, April MD, Naylor JF, et al. Prehospital Application of Hemostatic Agents in Iraq and Afghanistan. *Prehospital Emerg care Off J Natl Assoc EMS Physicians Natl Assoc State EMS Dir*. 2018;22(5):614-623. doi:10.1080/10903127.2017.1423140
9. Schauer SG, April MD, Naylor JF, et al. QuikClot® Combat Gauze® Use by Ground Forces in Afghanistan The Prehospital Trauma Registry Experience. *J Spec Oper Med a peer Rev J SOF Med Prof*. 2017;17(2):101-106.
10. Mueller GR, Pineda TJ, Xie HX, et al. A novel sponge-based wound stasis dressing to treat lethal noncompressible hemorrhage. In: *Journal of Trauma and Acute Care Surgery*. Vol 73. ; 2012. doi:10.1097/TA.0b013e3182617c3c
11. FDA. *De Novo Classification Request for XStat*.; 2013.
12. Kragh Jr. JF, Aden JK, Steinbaugh J, Bullard M, Dubick MA. Gauze vs XSTAT in wound packing for hemorrhage control. *Am J Emerg Med*. 2015;33(7):974-976. doi:10.1016/j.ajem.2015.03.048
13. Mann CT, Fischer H. *Recent Trends in Active-Duty Military Deaths* .; 2019. www.crs.gov%7C7-5700. Accessed March 19, 2020.
14. Pusateri AE, Modrow HE, Harris RA, et al. Advanced hemostatic dressing development program: animal model selection criteria and results of a study of nine hemostatic dressings in a model of severe large venous hemorrhage and hepatic injury in Swine. *J Trauma*. 2003;55(3):518-526. doi:10.1097/01.TA.0000075336.92129.27
15. Weaver FA, Hood DB, Zatina M, Messina L, Badduke B. Gelatin-thrombin-based hemostatic sealant for intraoperative bleeding in vascular surgery. *Ann Vasc Surg*. 2002;16(3):286-293. doi:10.1007/s10016-001-0073-0
16. Kheirabadi BS, MacE JE, Terrazas IB, et al. Safety evaluation of new hemostatic agents, smectite granules, and kaolin-coated gauze in a vascular injury wound model in swine. *J Trauma - Inj Infect Crit Care*. 2010;68(2):269-277. doi:10.1097/TA.0b013e3181c97ef1
17. Feng C, Li J, Wu GS, et al. Chitosan-Coated Diatom Silica as Hemostatic Agent for Hemorrhage Control. *ACS Appl Mater Interfaces*. 2016;8(50):34234-34243. doi:10.1021/acsami.6b12317
18. Ashokkumar S, Manimaran K, Kim K. Cultivation and Identification of Microalgae (Diatom). In: *Marine Algae Extracts*. Vol 1-2. Weinheim, Germany: Wiley-VCH Verlag GmbH & Co. KGaA; 2015:59-78. doi:10.1002/9783527679577.ch4
19. Sakoda M, Kaneko M, Ohta S, et al. Injectable Hemostat Composed of a Polyphosphate-Conjugated Hyaluronan Hydrogel. *Biomacromolecules*. 2018;19(8):3280-3290. doi:10.1021/acs.biomac.8b00588
20. Kumar VA, Wickremasinghe NC, Shi S, Hartgerink JD. Nanofibrous snake venom hemostat. *ACS Biomater Sci Eng*. 2015;1(12):1300-1305. doi:10.1021/acsbiomaterials.5b00356
21. Lendlein A, Kelch S. Shape-memory effect from permanent shape. *Angew Chem Int Ed Engl*. 2002;41:2034-2057.
22. Wilson TS, Bearinger JP, Herberg JL, et al. Shape memory polymers based on uniform aliphatic urethane networks. *J Appl Polym Sci*. 2007;106(1):540-551. doi:10.1002/app.26593

REFERENCES CITED

23. Rodriguez JN, Miller MW, Boyle A, et al. Reticulation of low density shape memory polymer foam with an in vivo demonstration of vascular occlusion. *J Mech Behav Biomed Mater*. 2014;40:102-114. doi:10.1016/j.jmbbm.2014.07.037
24. Rodriguez JN, Clubb FJ, Wilson TS, et al. In vivo response to an implanted shape memory polyurethane foam in a porcine aneurysm model. *J Biomed Mater Res - Part A*. 2014;102(5):1231-1242. doi:10.1002/jbm.a.34782
25. Landsman TL, Bush RL, Glowczwski A, et al. Design and verification of a shape memory polymer peripheral occlusion device. *J Mech Behav Biomed Mater*. 2016;63:195-206. doi:10.1016/J.JMBBM.2016.06.019
26. Rodriguez JN, Miller MW, Boyle A, et al. Reticulation of low density shape memory polymer foam with an in vivo demonstration of vascular occlusion. *J Mech Behav Biomed Mater*. 2014;40:102-114. doi:https://doi.org/10.1016/j.jmbbm.2014.07.037
27. Pusateri AE, Delgado A V, Dick EJ, Martinez RS, Holcomb JB, Ryan KL. Application of a granular mineral-based hemostatic agent (QuikClot) to reduce blood loss after grade V liver injury in swine. *J Trauma - Inj Infect Crit Care*. 2004;57(3):555-562. doi:10.1097/01.TA.0000136155.97758.CD
28. Tinkoff G, Esposito TJ, Reed J, et al. American association for the surgery of trauma organ injury scale I: spleen, liver, and kidney, validation based on the national trauma data bank. *J Am Coll Surg*. 2008;207(5):646-655. doi:10.1016/j.jamcollsurg.2008.06.342
29. Staikou C, Paraskeva A, Drakos E, et al. Impact of graded hypothermia on coagulation and fibrinolysis. *J Surg Res*. 2011;167(1):125-130. doi:10.1016/j.jss.2009.07.037
30. Christmas N, Vakil AU, Hatch CJ, et al. Characterization of shape memory polymer foam hemostats in in vitro hemorrhagic wound models. *J Biomed Mater Res Part B Appl Biomater*. 2021;109(5):681-692. doi:10.1002/jbm.b.34732
31. Hoyt DB, Bulger EM, Knudson MM, et al. Death in the operating room: an analysis of a multi-center experience. *J Trauma*. 1994;37(3):426-432. http://www.ncbi.nlm.nih.gov/pubmed/8083904. Accessed October 25, 2019.
32. Keenan S, Riesberg JC. Prolonged Field Care: Beyond the “Golden Hour”. *Wilderness Environ Med*. 2017;28(2S):S135-S139. doi:10.1016/j.wem.2017.02.001
33. Margolis J. Initiation of blood coagulation by glass and related surfaces. *J Physiol*. 1957;137(1):95-109. doi:10.1113/jphysiol.1957.sp005799
34. Horn JD, Maitland DJ, Hartman J, Ortega JM. Computational study of clot formation in aneurysms treated with shape memory polymer foam. *Med Eng Phys*. 2020;75:65-71. doi:10.1016/j.medengphy.2019.10.002
35. Muschenborn AD, Ortega JM, Szafron JM, Szafron DJ, Maitland DJ. Porous media properties of reticulated shape memory polymer foams and mock embolic coils for aneurysm treatment. *Biomed Eng Online*. 2013;12(1):103. doi:10.1186/1475-925X-12-103
36. Nash LD, Docherty NC, Monroe MBB, et al. Cold Plasma Reticulation of Shape Memory Embolic Tissue Scaffolds. *Macromol Rapid Commun*. 2016;37(23):1945-1951. doi:10.1002/marc.201600268

ACS APPLIED BIO MATERIALS

www.acsabm.org Article

Shape Memory Polymer Foams with Tunable Degradation Profiles

Anand Utpal Vakil, Natalie Marie Petryk, Ellen Shepherd, Henry T. Beaman, Priya S. Ganesh, Katheryn S. Dong, and Mary Beth B. Monroe*

Cite This: https://doi.org/10.1021/acsabm.1c00516 Read Online

ACCESS | Metrics & More | Article Recommendations | Supporting Information

ABSTRACT: Uncontrolled hemorrhage is the leading cause of preventable death on the battlefield and results in ~1.5 million deaths each year. The primary current treatment options are gauze and/or tourniquets, which are ineffective for up to 80% of wounds. Additionally, most hemostatic materials must be removed from the patient within <12 h, which limits their applicability in remote scenarios and can cause additional bleeding upon removal. Here, degradable shape memory polymer (SMP) foams were synthesized to overcome these limitations. SMP foams were modified with oxidatively labile ether groups and hydrolytically labile ester groups to degrade after implantation. Foam physical, thermal, and shape memory properties were assessed along with cytocompatibility and blood interactions. Degradation profiles were obtained in vitro in oxidative and hydrolytic media (3% H_2O_2 (oxidation) and 0.1 M NaOH (hydrolysis) at 37 °C). The resulting foams had tunable, clinically relevant degradation rates, with complete mass loss within 30−60 days. These SMP foams have potential to provide an easy-to-use, shape-filling hemostatic dressing that can be left in place during traumatic wound healing with future potential use in regenerative medicine applications.

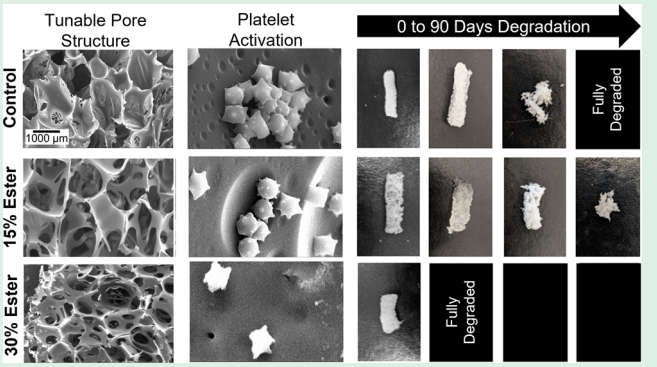

KEYWORDS: *shape memory polymers, polyurethanes, oxidation, degradation, foams*

1. INTRODUCTION

Hemorrhage is the leading cause of potentially survivable death on the battlefield. Up to 90% of preventable deaths are due to uncontrolled bleeding, and approximately 20% of combat casualties result in death before the injured can be transported to a treatment facility.[1−3] The most common hemorrhage treatment includes the use of tourniquets and gauze coated with coagulants. However, gauze is often ineffective at promoting clotting, and improper or prolonged tourniquet use can lead to complications like nerve paralysis, limb ischemia, arrhythmias, and crush syndrome, which can result in amputation above the position of a tourniquet.[4,5] This urgent clinical need has led to the recent development of new options for hemorrhage control. For example, XStat is designed for bleeding control from junctional wounds.[6] XStat contains ~95 oxidized cellulose foam pieces that are injected into the wound using a syringe-like applicator, after which they expand and fill up the wound to apply pressure and induce clotting.[7] Each foam piece must be removed within 4 h to prevent ischemia, and XStat exhibits a 22-fold increase in removal time compared with gauze.[6,8] This removal process can also lead to rebleeds of surrounding tissues. Therefore, XStat may not be the best alternative to gauze in remote locations where access to a fixed care facility is limited.

To overcome limitations of current hemostatic dressing options, an ideal hemostatic material is biocompatible, promotes rapid blood clotting, and is degradable. A degradable hemostatic dressing could theoretically be left in place after application to degrade during healing, prolonging the time available to get a patient to a fixed facility and reducing rebleed risks upon removal. To that end, He et al. prepared oxidized regenerated cellulose (ORC) gauze.[9] In a rabbit liver and ear-artery injury, this material induced hemostasis and degraded fully within 21 days; however, the gauze was forcibly removed by the blood flow from the artery, which reduces its applicability in traumatic hemorrhage control. Dai et al. developed silver-exchanged calcium-doped mesoporous silica spheres for hemorrhage control.[10] The particles achieved hemostasis within 340 s and underwent a 40% weight loss over 42 days in vitro. However, these mesoporous particles have a recorded pore size of 3.2 nm, which is likely too small to facilitate tissue ingrowth.[11] Porous chitosan-based hemostatic microparticles were developed by Li et al.[12] The microspheres exhibit an increase in blood clotting with decreased surface

Received: May 4, 2021
Accepted: August 3, 2021

pore size and a 40% weight loss over 4 weeks of lysozyme incubation but have a pore size of <2 μm. Thus, these microparticles may not be suitable for deep wounds to aid tissue ingrowth.

To address this clinical need, shape memory polymer (SMP) foams are being investigated as hemostatic biomaterials.[13] SMPs are "smart" stimuli-responsive materials that are synthesized in a primary, permanent shape, triggered using an external stimulus, such as heat or light, and strained/fixed into a temporary, secondary shape that is retained upon removal of the external stimulus. After re-exposure to the stimulus, SMPs regain their primary shape.[14] Heat is used as an external stimulus in this polyurethane SMP foam system, and shape change is designed around the polymer's glass-transition temperature (T_g). These foams are biocompatible and capable of promoting rapid blood clotting due to their thrombogenic surface chemistry and high surface area.[15,16]

The shape memory properties allow SMP foam radial compression and storage in a low-profile, temporary geometry at temperatures below their T_g. Foam T_g's are reduced by exposure to water (relative to T_g in dry conditions) due to plasticization of the polymer network.[17] Therefore, SMP foams can be stored compressed at relatively high temperatures (~40 to 50 °C) in the dry state. This smaller volume material can theoretically be packed into deep and/or irregularly shaped wounds, which is particularly important in gunshot wounds, which often have small entry points that expand outwards into large internal wound cavities.[18] Once exposed to water present in blood at body temperature (37 °C), the foam T_g is reduced, allowing expansion back to the original shape to fill up the space of wound, clotting the blood and reducing further hemorrhage. One of the main advantages of these foams over commercially available hemostatic materials is that their chemistry can be tuned according to application requirements. The goal of the current work is to modify the SMP foams to degrade after implantation to enable prolonged use and reduce rebleed risks during removal.

Weems et al. found that SMP foams undergo oxidative degradation via scission of tertiary amines in the monomers.[19] "Real-time" in vitro degradation studies in 3% H_2O_2 revealed a 50% mass loss over ~100 days. To increase the degradation rate, previous efforts focused on incorporating hydrolytically degradable ester linkages into the polymer network. Singhal et al. added poly(caprolactone) macromers into the system.[20] These foams had a relatively low T_g around 20 °C, which limits their stable storage in the secondary shape, and mass losses were slow, even in accelerated degradation media.[21] Weems et al. synthesized succinic acid-based ester-containing foams with higher T_g.[22] However, degradable formulations still had relatively low dry T_g (~37 °C) and mass loss rates that are slower than wound healing rates (complete mass loss in 80 days in 2% H_2O_2). To improve upon this system, degradable SMP foams with appropriate thermal properties (T_g > 50 °C) were developed by Jang et al. using ester-containing trifunctional monomers.[23] However, the fastest complete mass loss was observed within 90 days in an accelerated oxidative degradation medium (20% H_2O_2). Thus, SMP foams with appropriate thermal properties and more rapid degradation rates to better match tissue regeneration are still required.

Due to the hydrophobicity of the foams, we hypothesized that clinically relevant degradation rates (~6 to 8 weeks based on previous clinical data[24]) could be obtained by increasing the local hydrophilicity around hydrolytically degradable ester groups. To that end, we synthesized new monomers by esterifying nitrilotriacetic acid (NTA) with diethylene glycol (DEG) and incorporated the resulting ester-containing monomer into SMP foams. NTA includes an oxidatively degradable tertiary amine, DEG increases hydrophilicity next to the hydrolytically degradable ester linkages, and the ether linkages of DEG are susceptible to oxidative degradation.[20] After characterizing scaffold properties, cytocompatibility, and blood interactions, degradation was assessed in 3% H_2O_2 at 37 °C to mimic real-time oxidative degradation in the body and in an accelerated hydrolytic degradation solution (0.1 M NaOH).[25,26] Mass loss, pore size/structure, surface chemistry, and T_g were measured over time to establish in vitro degradation profiles. These SMPs have the potential to provide an easy-to-use, shape-filling hemostatic dressing that can be left in place during traumatic wound healing.

2. MATERIALS AND METHODS

2.1. Materials. Hydrogen peroxide (H_2O_2, certified ACS, 30%), sodium hydroxide (NaOH), ethanol (reagent alcohol), chloroform, nitrilotriacetic acid (NTA), 1-(3-dimethylaminopropyl)-3-ethylcarbodimide HCl (EDC), 4-(dimethylamino)pyridine (DMAP, ≥99%), hexamethylene diisocyanate (HDI), N,N,N′,N′-tetrakis-(2-hydroxypropyl)-ethylenediamine (HPED), triethanolamine (TEA), diethylene glycol (DEG), Triton X-100, and phosphate-buffered saline (PBS) were purchased from Fisher Scientific (Waltham, MA) and used as received. Porcine blood was purchased from Lampire Biological Laboratories (Pipersville, PA). Glutaraldehyde was purchased from Electron Microscopy Sciences (Hatfield, PA). EPH-190, BL-22, and T-131 were provided by Evonik (Essen, Germany) and used as received.

2.2. Synthesis of Ester-Containing Triol. NTA and DEG were added to chloroform at a 1:3 molar ratio with 0.1 mol. equiv of DMAP and 3 mol. equiv of EDC as catalysts (Figure 1). The reaction was carried out at 40 °C in a nitrogen environment over molecular sieves, which were added to capture water produced during the esterification reaction. Attenuated total reflectance Fourier transform infrared spectroscopy (ATR-FTIR, Nicolet iS10, Thermo Scientific) was carried out on the reaction product every 24 h to track its completion according to the introduction of a peak at ~1714 cm^{-1} that corresponds with the C═O of the ester. Upon reaction

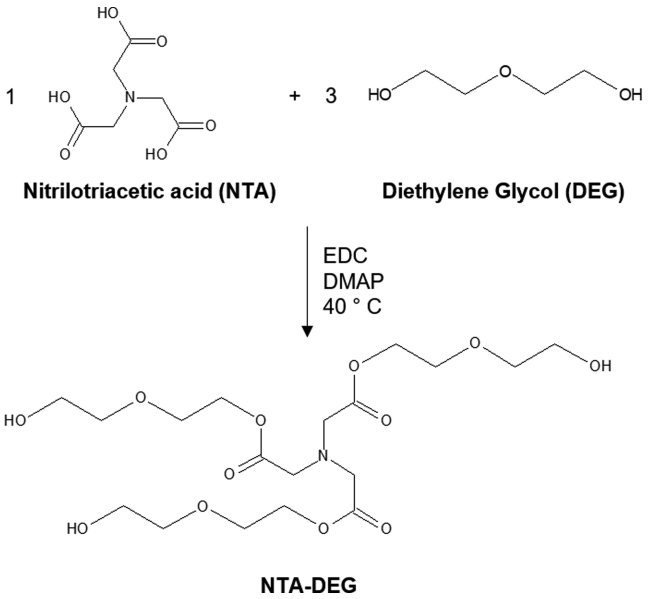

Figure 1. Synthesis of ester-containing monomer, nitrilotriacetic acid (NTA)−diethylene glycol (DEG).

Table 1. Synthesized Foam Compositions

sample ID	HDI (wt %)	HPED (wt %)	TEA (wt %)	DEG (wt %)	NTA−DEG (wt %)	EPH-190 (wt %)	T-131 (wt %)	BL-22 (wt %)	water (wt %)
Control	54.03	27.61	8.05			6.44	0.46	1.01	2.37
15% NTA−DEG	49.45	25.27		3.93	11.23	6.44	1.20	1.01	2.40
30% NTA−DEG	43.10	24.40			21.71	6.17	1.10	1.23	2.29

completion, excess solvent was vaporized using rotary evaporation, and the final product was dried overnight under vacuum. The dried product, NTA−DEG, was analyzed using ATR-FTIR and ^{1}H-nuclear magnetic resonance (NMR, Bruker Avance III HD 400 MHz) spectroscopy to confirm the formation of ester linkages. Successful esterification of DEG was indicated by an ester peak at 1741 cm^{-1} in the FTIR spectra (Figure S1a). NMR spectra were collected in $CDCl_3$ at 298 K using the TMS/solvent signal as an internal reference. NTA−DEG: ^{1}H NMR ($CDCl_3$; ppm): 3.64 (t, $-CH_2CH_2OCO-$), 3.64 (t, $-CH_2OH$), 3.72 (s, $-CH_2N-$), 3.78 (t, $-CH_2CH_2OH$), and 4.25 (s, $-CH_2OCO-$). NMR confirmed 85−88% functionalization of NTA carboxylic acids with DEG (Figure S1b).

2.3. Foam Synthesis. Polyurethane foams were fabricated using a two-step process. In the first step, an isocyanate (NCO) premix was prepared that contained 100 mol % of required isocyanates from HDI and a fraction of hydroxyl equivalents from HPED, TEA, and NTA−DEG. The premix was reacted at 50 °C for 48 h. The remaining mol % of hydroxyl components was mixed with catalysts (T-131 and BL-22) and a blowing agent (deionized (DI) water). Surfactant (EPH-190) was added to the premix after the 48 h cure. The NCO premix and hydroxyl components were mixed in a high-speed mixer (Flacktek, Landrum, SC) and poured into a large beaker, which was incubated at 50 °C for 5−10 min to allow for foam formation. Synthesized foam compositions are shown in Table 1.

2.4. Foam Pore Analysis. Pore sizes of samples were measured using scanning electron microscopy (SEM). Samples (n = 3, 1 cm^2) were cut along the vertical and lateral foam axes and sputter-coated with gold using a Denton Vacuum sputter coater before imaging (Jeol JSM 5600) at 35× magnification and a 10 kV high vacuum. The micrographs were analyzed using ImageJ software to quantify pore diameters.

2.5. Density. Samples (n = 3) were cut into cubes (1 cm^3) using a hot wire cutter, and the length of each face was measured using digital calipers. Measurements were converted to volumes, and samples were then weighed to determine densities.

2.6. Mechanical Testing. Samples (n = 3) were cut in dog bone shapes (ASTM D638 scaled down by a factor of 4) with a gauge length of 6.25 mm and a width of 1.5 mm. The samples were tested in both dry and wet conditions. To measure wet tensile properties, samples (n = 3) were placed in 50 °C DI water for 5 min and pressed dry prior to fixing on the tensile tester. Samples were placed into a tensile tester with a 24 N load cell and stretched at a rate of 2 mm/min until failure to measure elastic modulus, elongation at break, and ultimate tensile strength.

2.7. Thermal Analysis. A Q200 differential scanning calorimeter (DSC, TA Instruments, New Castle, DE) was used to measure T_g. Samples (n = 3, 3−5 mg) were placed in t-zero aluminum pans and then equilibrated at −40 °C, heated to 120 °C at 10 °C/min, kept isothermally for 2 min, cooled to −40 °C, kept isothermally for 2 min, and heated to 120 °C at 10 °C/min. Dry T_g was measured as the half-height transition temperature during the second heating cycle. To measure wet T_g, samples (n = 3) were placed in 50 °C DI water for 5 min, pressed dry, and placed in t-zero aluminum pans prior to running a single heating cycle.

2.8. Swelling Ratio. Cylindrical foam samples (~20 to 30 mg in dry weight) were cut, cleaned in DI water and 70% ethanol, and dried under vacuum at 40 °C. Their dry masses (W_d) were obtained (n = 3), and then they were placed in 37 °C water for 5 min or 24 h. Samples were patted dry on a laboratory wipe and then weighed to obtain swollen masses (W_w). Swelling ratio (SR) was calculated as

$$\mathrm{SR} = \frac{W_w - W_d}{W_d} \times 100\%$$

2.9. Shape Memory Behavior. Cylindrical foam samples (1 cm length, 8 mm diameter) were cut, cleaned in DI water and 70% ethanol, and dried under vacuum at 40 °C. Cleaned samples were heated to 100 °C for 10 min. The diameter (n = 3) was measured using digital calipers prior to crimping cylinders in a radial compression crimper (Blockwise Engineering, Tempe, AZ) and cooling them down while crimped. Crimped samples were placed in vials in a dry box containing a desiccant for 24 h and then fixed on a 330 μm Nitinol wire. Their diameters were measured again, and then they were placed in a DI water bath at 37 °C. Expansion profiles were captured using a camera that recorded images every 5 s for 5 min. The images were processed using Insight Toolkit (ITK) to measure the change in diameter over time. Foam area (number of pixels) from each image was normalized against that of the last image with the known diameter (measured using calipers after foam was removed from the water bath), and % volume recovery was calculated as

$$\%\ \text{volume recovery} = \frac{\text{sample diameter}(t)}{\text{initial diameter}} \times 100\%$$

Foam diameter vs time was plotted over the expansion time frame.

2.10. Spectroscopic Analysis. Surface chemistry of foams was characterized by collecting ATR-FTIR spectra on thin slices of foam at a 0.8 cm^{-1} resolution.

2.11. Cytocompatibility. NIH/3T3 Swiss mouse fibroblasts (ATCC−CCL92) were cultured with Dulbecco's modified Eagle's medium (DMEM, high glucose GlutaMAX) supplemented with 10% heat-inactivated fetal bovine serum (FBS) and 1% penicillin−streptomycin (P/S, Gibco) at 37 °C/5% CO_2. For all studies, cells (between passages 4 and 6) were used after 3 days of culture. Cells were seeded in a 24-well tissue-culture polystyrene plate at 10,000 cells/well and cultured for 24 h. Morphology was assessed using a Zeiss Axiovert inverted microscope to confirm even cell distribution. Media was removed, and cells were washed with sterile phosphate-buffered saline (PBS) prior to exposure to samples. Then, the cleaned foam pieces were placed in Transwell inserts in the preseeded plates along with fresh DMEM with 10% FBS and 1% P/S. Positive (cytocompatible) controls included wells with empty inserts, and negative (cytotoxic) controls included wells with empty inserts and 0.5% H_2O_2 in media.

Following incubation over 3, 24, and 72 h, a Resazurin cell viability assay was utilized to quantify cytocompatibility. Transwell inserts and solutions were removed from wells and replaced with the Resazurin cell viability stain for 4 h at 37 °C. Then, a plate reader (FLx800, BioTek Instruments, Inc.) was used to measure absorbance at 570 nm. Cell viability was calculated as

$$\text{cell viability}\ (x) = \frac{\mathrm{abs}_{570}(x)}{\mathrm{abs}_{\text{control}}} \times 100\%$$

where x is the selected treatment group, and the empty insert control is used as a standard that equals 100% viability.

2.12. Blood Interactions. Porcine blood (Lampire Biological Laboratories, Pipersville, PA) anticoagulated with Na-citrate upon collection was stored at 4 °C for up to 3 weeks from the bleed date. Control, 15% NTA−DEG, and 30% NTA−DEG foams were washed and dried prior to characterization in all studies. QuikClot Combat Gauze was included as a clinical control. Blood absorption was analyzed by weighing dried samples (n = 3; ~50 mg) and incubating

https://doi.org/10.1021/acsabm.1c00516
ACS Appl. Bio Mater. XXXX, XXX, XXX−XXX

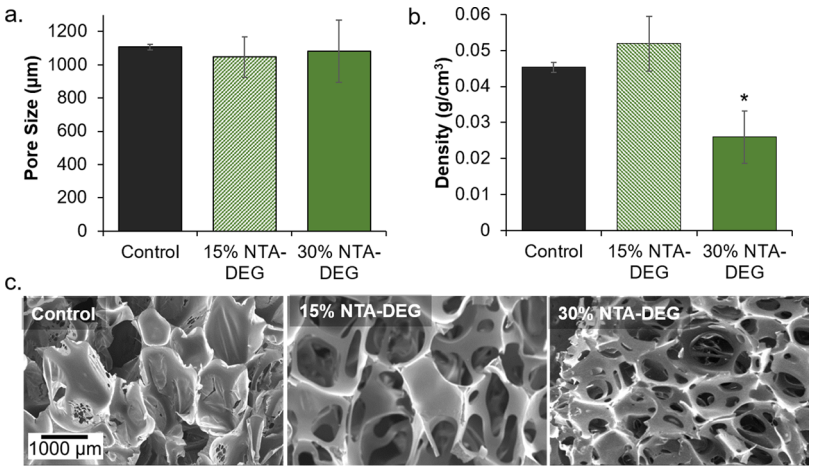

Figure 2. Structural properties of synthesized foams. (a) Average pore size of foams (n = 6) measured using SEM micrographs and subsequent SEM analysis. (b) Foam densities (n = 3). (c) Representative SEM micrographs of foam samples used for pore analysis. Scale bar of 1000 μm applies to all images. Average ± standard deviation displayed in panels (a) and (b). *p < 0.05 relative to control foam.

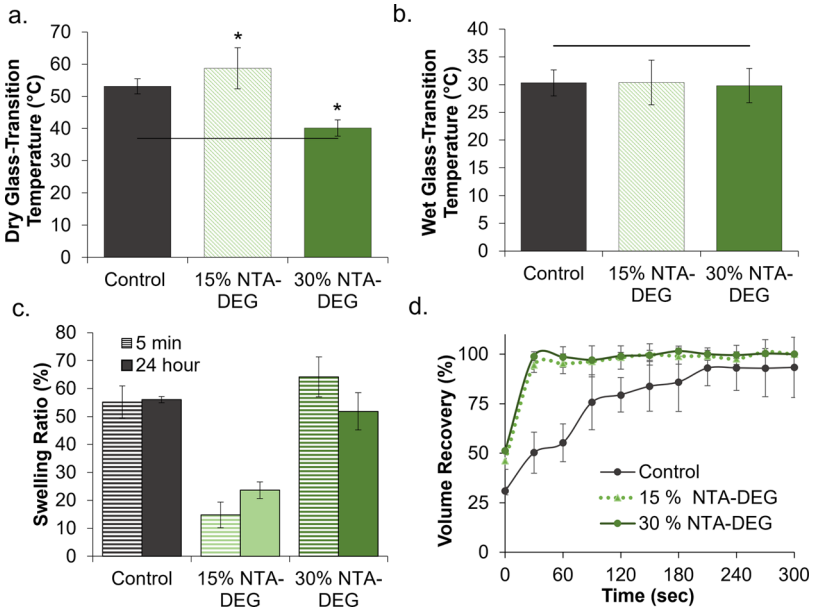

Figure 3. Thermal and shape memory properties of SMP foams. T_g measured via differential scanning calorimetry under (a) dry and (b) wet conditions (n = 3). *p < 0.05 relative to control. Horizontal lines indicate body temperature (37 °C). (c) Volumetric swelling ratios in water at 5 min and 24 h at 37 °C (n = 3). (d) Volume recovery profiles of foam samples in deionized water at 37 °C (n = 3). Average ± standard deviation displayed for all data.

them in blood at 37 °C. Samples were weighed at 24 h, and blood absorption was calculated as

$$\% \text{ absorbed} = \frac{W_b - W_d}{W_d} \times 100\%$$

where W_b is the mass of the sample in blood and W_d is the dry mass.

Coagulation time was measured by placing samples (n = 4) in 1.5 mL tubes, with empty tubes serving as negative (nonclotting) controls. Blood was brought to room temperature, and a 1 M $CaCl_2$ solution was added to obtain a final concentration of 0.01 M $CaCl_2$ and reverse the anticoagulant. Then, 50 μL of blood was added to each sample tube. At each time point (every 6 min over 30 min), 1 mL of DI water was added to the tubes to stop the clotting process and lyse free red blood cells. Tubes were centrifuged (2300 rpm, 15 min), inverted, and imaged using a digital camera. Then, 200 μL of lysate was pipetted from each tube into a 96-well plate, and absorbance was measured at 540 nm using a BioTek Synergy 2 Multi-Mode Microplate Reader (Winooski, VT) to determine the relative amount of hemoglobin released at each time point.

2.13. Platelet Attachment. An LDH cytotoxicity assay kit (Cayman Chemical, Ann Arbor, MI) was used to quantify the attachment of platelets to samples. To obtain a standard curve, whole blood was centrifuged at 3000 rpm for 15 min to obtain platelet-rich plasma (PRP). Multiple concentrations of PRP were prepared by diluting with PBS at 100, 50, 25, 12.5, and 6.5% to generate a standard. Hemocytometer counts at each PRP concentrations (n = 4) were acquired and used to quantify standard values.

SMP foams (n = 4) were cut to have equal surface areas and placed in the wells of a 24-well plate. Gauze was used as a clinical control. Then, 1 mL of whole blood was added to each well and the plate was incubated at 37 °C for 30 min. Nonattached platelets were washed away with PBS. Samples were transferred to another plate containing 1 mL of fresh PBS and 100 μL of 10% Triton X-100 and incubated at 37 °C for 1 h to lyse the attached platelets. Then, 100 μL of supernatant was taken from each sample well and transferred to a 96-

Table 2. Tensile Properties of Shape Memory Polymer Foams in Dry and Wet Conditions[a]

	dry			wet		
sample	elastic modulus (kPa)	ultimate tensile strength (kPa)	maximum elongation (mm/m)	elastic modulus (kPa)	ultimate tensile strength (kPa)	maximum elongation (mm/m)
Control	3216 ± 1669	528 ± 230	0.17 ± 0.04	153 ± 22	53 ± 21	0.36 ± 0.19
15% NTA–DEG	217 ± 86*	69 ± 26*	0.39 ± 0.20	24 ± 5*	45 ± 20	1.73 ± 0.39
30% NTA–DEG	78 ± 33*	94 ± 7*	1.39 ± 0.60*	15 ± 3*	70 ± 24	4.53 ± 1.34*

[a] n = 3, average ± standard deviation displayed. *p < 0.05 relative to control.

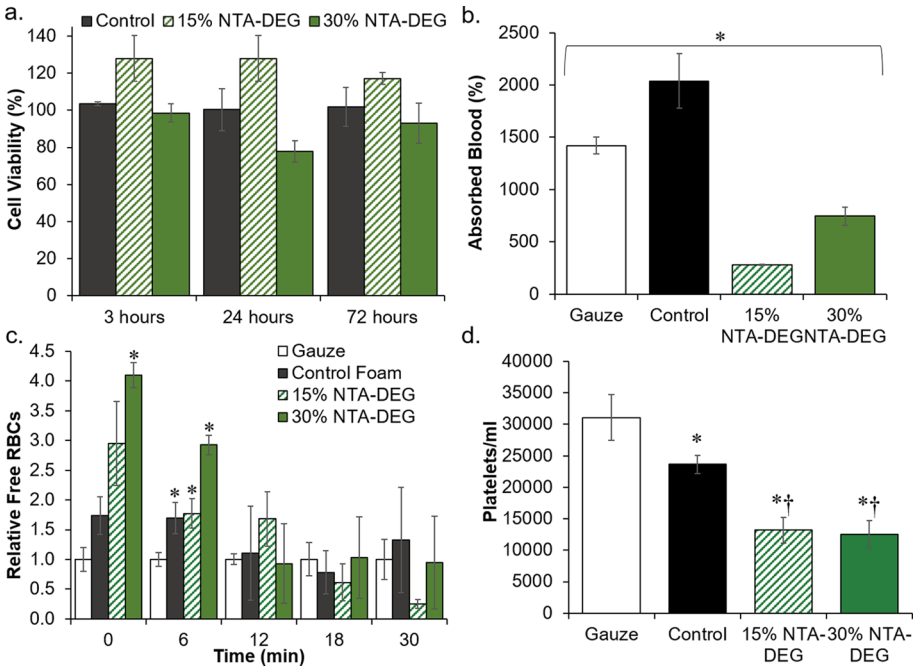

Figure 4. Cell and blood interactions with SMP foams. (a) 3T3 fibroblast viability over 3, 24, and 72 h (n = 3). (b) Blood absorption over 24 h at 37 °C (n = 3). *p < 0.05 between all four samples. (c) Blood clotting times in terms of free red blood cells (RBCs) relative to gauze clinical control over 30 min (n = 4). *p < 0.05 relative to gauze. (d) Platelet attachment concentrations measured using the LDH assay (n = 4). *p < 0.05 relative to gauze. †p < 0.05 relative to control foam. Average ± standard deviation displayed for all data.

well plate. The LDH reaction solution (100 μL) was added to each well, and the plate was incubated for 30 min at 37 °C on an orbital shaker. Following incubation, absorbances were read on the microplate reader at 490 nm.

2.14. Platelet Activation. SMP foams (approximately 0.5 cm^3) were incubated in whole blood and rinsed of nonattached platelets. To observe activity states and activation of the attached platelets, samples were prepared for SEM imaging. Samples were fixed in a solution of 2% glutaraldehyde (Electron Microscopy Sciences, Hatfield, PA) overnight at 4 °C. Following fixation, samples were dehydrated in solutions with increasing concentrations of ethanol: (1) 30 min in 50% ethanol, (2) 30 min in 70% ethanol, (3) 30 min in 95% ethanol, and (4) 30 min in 100% ethanol. The final dehydration was accomplished through drying overnight in a vacuum oven at room temperature, and samples were sputter-coated with 5–10 nm of gold. SEM analysis was performed using a Jeol NeoSCope JCM-5000 scanning electron microscope at an operating voltage of 10 kV. Random regions of interest were imaged at 1000× and 5000× magnifications. Images were analyzed qualitatively for signs of platelet aggregation and morphology change.

2.15. Degradation Analysis. Cylindrical foams (n = 8, 8 mm diameter, 1 cm height) were washed and dried, and initial masses were obtained using a gravimetric scale. Samples were placed in 3% H_2O_2 (real-time oxidative degradation media) or in 0.1 M NaOH (accelerated hydrolytic degradation media) at 37 °C. Every 3 days, the degradation media was changed. At selected time points, samples were washed with ethanol and dried under vacuum for 24 h. After drying, samples were imaged using a camera, and masses were measured (n = 5). A thin slice was cut from a sacrificial set of foams (n = 3) and used to measure pore morphology, T_g, and surface chemistry as described above.

2.16. Statistical Analysis. Measurements are presented as mean ± standard deviations. Student's t tests were performed to determine differences between NTA–DEG foams and controls. Statistical significance was taken as p < 0.05.

3. RESULTS

3.1. Structural Properties. All formulations had a pore size of approximately 1100 μm, and both NTA–DEG formulations had comparable pore sizes to the control (Figure 2). In general, foam densities were low (<0.06 g/cm^3) for all formulations, demonstrating that the NTA–DEG monomer can be incorporated into low-density foams. The addition of NTA–DEG resulted in pore opening, with interconnects visible in pore walls (Figure 2c), which corresponds with a significantly reduced density in the 30% NTA–DEG foams relative to that of the control foam.

3.2. Thermal Properties. The use of polyol cross-linkers with three (TEA and NTA–DEG) and four (HPED) hydroxyl groups provides an amorphous, highly cross-linked network

https://doi.org/10.1021/acsabm.1c00516
ACS Appl. Bio Mater. XXXX, XXX, XXX–XXX

that is indicated by the absence of melting peaks in the DSC plots. The shape memory properties are designed around the dry and wet T_g's of the system. Figure 3a shows that all foam formulations have dry T_g's over 40°C, which ensures that the biomaterials maintain their compressed secondary shape when stored in dry conditions. The wet T_g's are reduced to below 37 °C due to plasticization of the network by water, as shown in Figure 3b, which allows for the actuation of shape memory properties after exposure to water in body-temperature blood upon implantation.

3.3. Hydrophilicity and Shape Memory Behavior. Swelling ratios in water were calculated to provide an indication of material hydrophilicity (Figure 3c). Control foams swelled by 55% in 5 min, and the effective swelling after 24 h was 56%. Similarly, 30% NTA−DEG swelled by 64% in 5 min and 51% in 24 h, while 15% NTA−DEG swelled a significantly lower amount of 15% in 5 min and 23% in 24 h. The statistically similar swelling ratios at the 5 min and 24 h time points indicate that equilibrium swelling is reached within the first 5 min of water incubation with these foams. Shape memory properties of foams are required to ensure that they expand to their original shape after implantation and exposure to body-temperature blood. The volume recovery profiles of the foams in water at 37 °C are shown in Figure 3d. Control foams expanded back to their original shape within ∼200 s, while NTA−DEG foams reached a 100% volume recovery within ∼25 s.

3.4. Tensile Testing. Mechanical testing data are presented in Table 2. In general, elastic modulus and tensile strength decreased and maximum elongation increased with the addition of NTA−DEG. These trends were observed in both dry and wet/plasticized conditions. Relative differences in elastic modulus were reduced in wet conditions (15× and 41× decreases between control and 15 and 30% NTA−DEG, respectively, in dry condition vs 6× and 10× decreases in wet condition). Tensile strength was similar between samples in the wet state, and ultimate elongation differences increased in wet conditions.

3.5. Cell and Blood Interactions. Cell viability was >75% for all samples over 72 h (Figure 4a). Control foams absorbed significantly more blood than gauze and NTA−DEG foams (Figure 4b). The lowest blood absorption was measured in 15% NTA−DEG foams, followed by 30% NTA−DEG foams. Clotting times were measured relative to a gauze clinical control (Figure 4c). At 6 min, all SMP foams had significantly higher free red blood cells (RBCs) relative to the gauze clinical control, indicative of reduced clotting. However, by 12 min, all samples had comparable clotting levels. Images of lysates can be viewed in Figure S2 in the Supporting Information.

3.6. Platelet Attachment and Activation. Decreasing concentrations of PRP resulted in a linear decrease in platelet numbers that could be used to quantify the concentrations of attached platelets on samples using the LDH assay. As shown in Figure 4d, the highest levels of platelet attachment were observed on the gauze clinical control, followed by the SMP control foam. Ester-containing foams had a significantly lower concentration of attached platelets compared to that of the controls. Platelets were found on all materials in SEM images. The granules released from the cytoplasm of platelets upon activation after attachment can be visualized by the small protrusions seen in Figure 5. The gauze clinical control contained areas of thrombus formation, indicating that platelets attached, aggregated, and activated during the 30 min of whole blood incubation. All SMP formulations showed evidence of platelet attachment and activation. Aggregates were found on control and 15% NTA−DEG samples, while 30% NTA−DEG samples had lower platelet density.

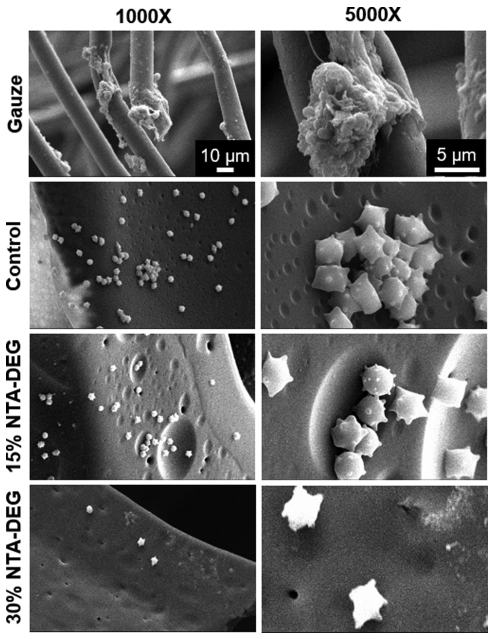

Figure 5. SEM micrographs of attached and activated platelets after incubation in whole porcine blood. Scale bars apply to all images in a given column.

3.7. Degradation Analysis. *3.7.1. Mass Loss and Physical Erosion.* Despite the inclusion of hydrolytically degradable ester linkages, NTA−DEG foams were relatively stable in 0.1 M NaOH (Figure 6b). They lost ∼20% of their mass within 1−2 weeks, after which mass loss plateaued. The remainder of the hydrolytic degradation characterization data

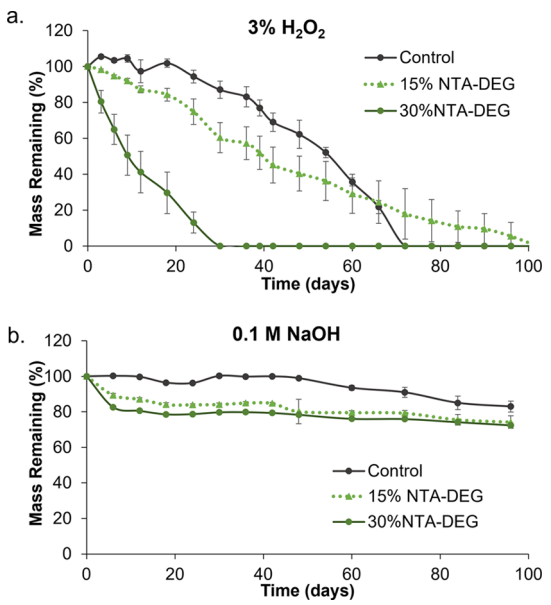

Figure 6. Mass loss of samples as a function of time (n = 5) in (a) real-time oxidative degradation media (3% H_2O_2) and (b) accelerated hydrolytic degradation media (0.1 M NaOH). Average ± standard deviation displayed.

https://doi.org/10.1021/acsabm.1c00516
ACS Appl. Bio Mater. XXXX, XXX, XXX−XXX

can be found in Figures S3–S5 in the Supporting Information. In 3% H_2O_2, the 30% NTA–DEG foams underwent linear mass loss (R^2 = 0.953) over 30 days (Figure 6a). The 15% NTA–DEG foams had a consistent, linear mass loss (R^2 = 0.976) in 3% H_2O_2 with full degradation at 100 days. Control foams have initially slow degradation rates, and the rate increased around 42 days until 100% degradation within 72 days (R^2 = 0.894). In general, NTA–DEG foams remained in a single piece throughout the degradation process, which indicates that surface erosion occurred in these samples, while control foams started to break apart into smaller pieces after ~42 days (Figure 7).

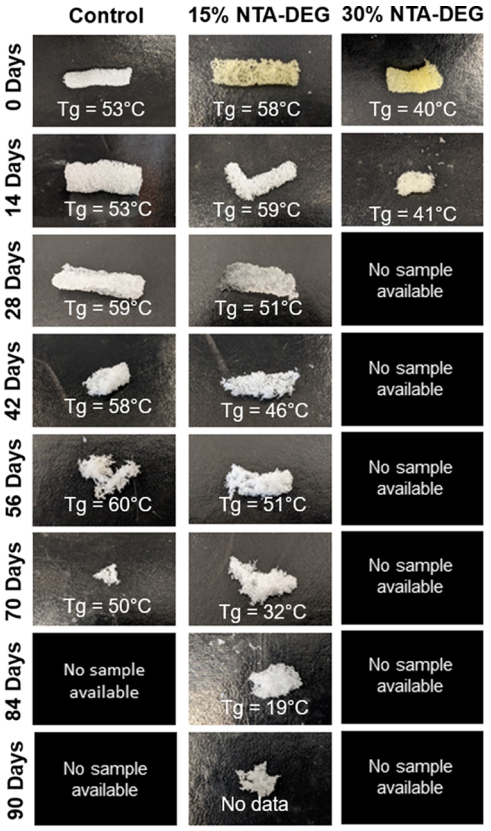

Figure 7. Erosion profile and glass-transition temperatures of samples during degradation in 3% H_2O_2. No sample was available for imaging upon almost complete degradation at ~28 days for 30% NTA–DEG foams and at ~84 days for controls.

3.7.2. Thermal Analysis. Variations in T_g throughout degradation provide an indication of relative cross-link densities over time. This information can be used to determine if the materials undergo bulk degradation, where the entire network is attacked at once, or surface degradation, where the network remains relatively stable.[27−29] Retained T_g's throughout the degradation time frame, as shown in Figure 7, indicate that the polymer networks remained fairly intact and that degradation occurred primarily on the surface of the materials. This is expected for oxidative degradation due to the high reactivity of reactive oxygen species.[30] The 15% NTA–DEG foam T_g dropped at 70 days, indicating that bulk hydrolysis may take over as the primary degradation mechanism at this point.[29]

3.7.3. Pore Morphology. Pore morphology of foams was observed every 2 weeks via SEM, as shown in Figure 8. In the

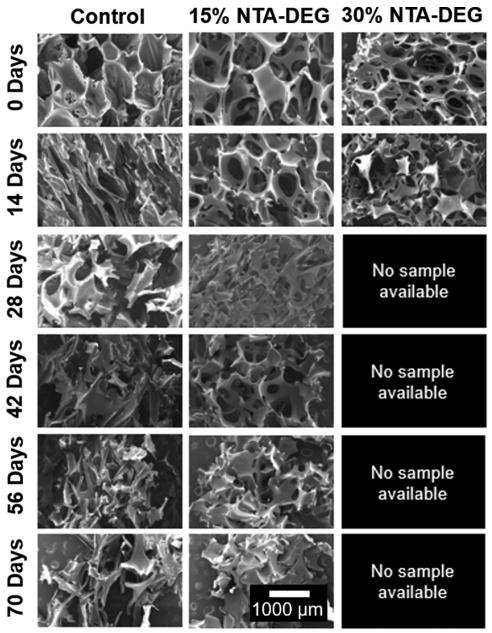

Figure 8. SEM micrographs of samples throughout 10 weeks of degradation in 3% H_2O_2. 30% NTA–DEG degraded completely by the 28 day time point. Scale bar of 1000 μm applies to all images.

case of control foams in 3% H_2O_2, the pores began to collapse by 14 days with significant strut breakage by 28 days. Total pore collapse at 42 days corresponds to the macroscale breaking apart of control foams shown in Figure 7. Pore morphology was the most stable in the 15% NTA–DEG foams, with visible pores and interconnects as late as 42 days, despite the increased mass loss in these samples in comparison with the controls (69 ± 5% remaining in control vs 45 ± 9% remaining in 15% NTA–DEG). The 30% NTA–DEG foams degraded too much for imaging by the 28 day time point, and evidence of significant degradation (loss of struts) can be seen by 14 days.

3.7.4. Spectroscopic Analysis. As seen in Figure 9, a shift in the carbonyl of urethane peak from 1680 to 1688 cm^{-1} and a reduction in the tertiary amine of HPED and TEA (and NTA for ester-containing foams) at 1050 cm^{-1} are an indication of oxidative degradation across all of the formulations, as previously shown.[19,23] Among the NTA–DEG foams, an increase in the carbonyl of the carboxylic acid peak at 1650 cm^{-1} is attributed to the carboxylic acid byproduct formation during hydrolytic cleaving of ester linkages.

4. DISCUSSION

4.1. Foam Characterization. The addition of NTA–DEG as a monomer aided in opening the pores, as demonstrated by pinholes in pore walls (Figure 2c). This increased interconnectivity between pores may be attributed to the hydrophilicity of DEG. Namely, the relatively hydrophilic DEG component increases interactions between the prepolymer/monomers and the water blowing agent and/or surfactant to aid in pore opening. Previous attempts to increase interconnectivity in SMP foams rely upon mechanical reticulation, plasma treatment, and/or use of physical blowing agents.[31,32] Inclusion of more hydrophilic monomers presents a new method for pore opening in these materials. This interconnectivity could increase nutrient transfer throughout the biomaterial scaffold, as well as allow for tissue and blood

https://doi.org/10.1021/acsabm.1c00516
ACS Appl. Bio Mater. XXXX, XXX, XXX–XXX

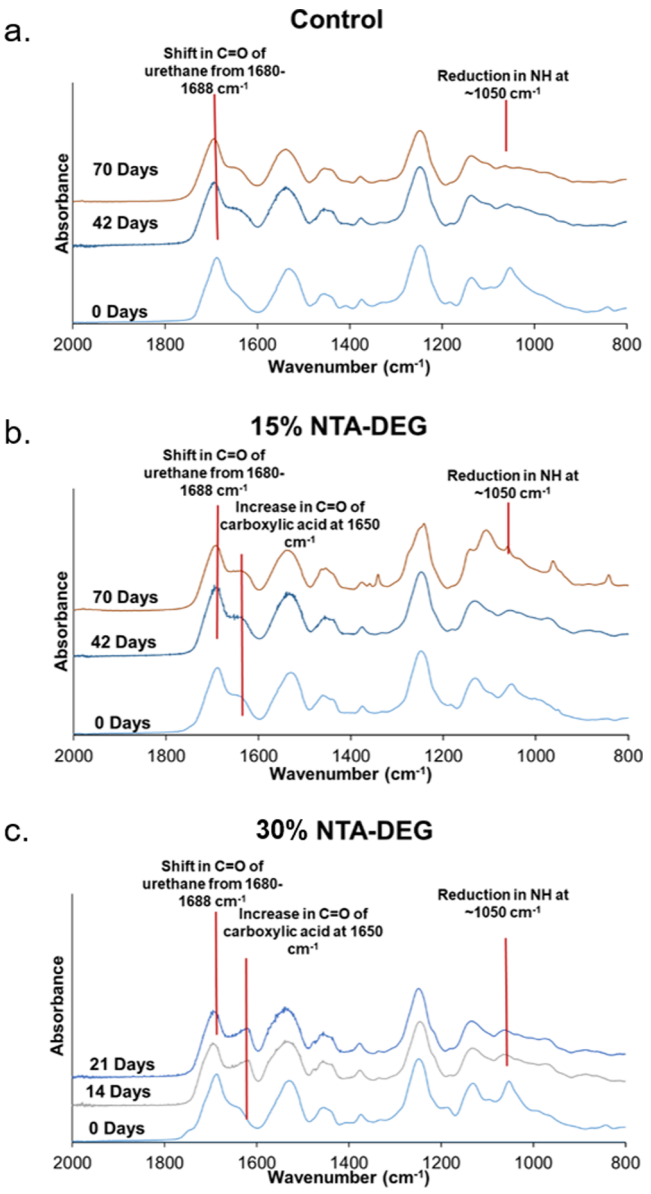

Figure 9. FTIR spectra of (a) control, (b) 15% NTA−DEG, and (c) 30% NTA−DEG throughout 10 weeks of degradation in 3% H_2O_2. 30% NTA−DEG degraded completely after the 21 day time point.

vessel ingrowth, and it expands potential future applications for SMP foams in tissue engineering and regenerative medicine applications.[33,34]

In general, SMPs contain two main components at the molecular level, known as net points and switching segments.[35] Net points define the permanent shape of the SMP. In this specific material system, the net points are covalent cross-links that form during synthesis (urethane linkages that form upon reaction with hydroxyls with isocyanates). Switching segments provide the mechanism for shape memory. In this specific system, the switching segments are hydrogen bonds that form between urethane linkages in between the cross-links. At temperatures above the T_g, hydrogen bonds are broken between the network chains to increase flexibility, making the material elastic. This elasticity allows for deformation (radial crimping in this case) into the secondary shape. Upon cooling below the T_g, new hydrogen bonds form between chains that have been rearranged during crimping, again limiting SMP flexibility and fixing the temporary shape. Upon exposure to body temperature water after shape fixation, the hydrogen bonds between the urethane linkages are interrupted by water plasticization that reduces the T_g and triggers shape recovery at a relatively lower temperature in the wet condition.

A reduction in dry T_g of 30% NTA−DEG foams can be attributed to the longer chain length and increased flexibility of NTA−DEG monomers, which theoretically reduces the overall cross-link density and network rigidity. Plasticization after exposure to water reduces the T_g in the wet state and enables actuation after exposure to body temperature (37 °C water). All foams have wet T_g below 37 °C. It was originally hypothesized that NTA−DEG foams may have lower wet T_g due to the hydrophilic DEG chains; however, wet T_g's were statistically similar for the three foam formulations. The retained wet T_g of NTA−DEG foams as compared to controls is attributed to intermolecular bonding between the dipoles of ester linkages.

Previous research on polyurethane foams shows that the materials primarily hydrogen-bond with water through the N−H groups rather than through the C═O linkages, based upon Fourier transform infrared (FTIR) spectra.[36] Namely, when hydrogen bonds form at the N−H groups, the N−H infrared band at ∼3307 cm^{-1} increases in intensity and shifts to higher wavenumbers. When hydrogen bonding occurs via bridges between two C═O groups, the FTIR spectra show an increase in the intensity of the C═O peak at ∼1687 cm^{-1} with shifts to lower wavenumbers. In the current study, we collected FTIR spectra on foams that had been submerged in water at 50 °C for 5 min and compared those with dry foam spectra (shown in Figure S6 in the Supporting Information). The N−H peak intensities increased with general shifts to higher wavenumbers in the wet foam spectra, indicating the presence of hydrogen bonds between water and the N−H groups in the urethane linkages. Meanwhile, the C═O peaks at ∼1687 cm^{-1} were of similar intensity between the wet and dry samples, with no apparent shift in wavenumber, indicating minimal hydrogen bonding between these groups in these materials. These FTIR spectra support the hypothesis that the dipole−dipole bonds in these foams are less susceptible to water plasticization via hydrogen bonding, which would correlate with reduced effects on wet T_g in this system.

This hypothesis also correlates with the foam swelling ratios in water. Namely, there is a drop in swelling in the 15% NTA−DEG foams that may be attributed to the dipole−dipole bonds with reduced water access. With an increase in the NTA−DEG content to 30%, the hydrophilicity of DEG overcomes these restrictions to increase water interactions with the network. The faster volume recovery observed with NTA−DEG foams is likely due to the open pore structure, which enables faster water penetration and shape recovery from the compressed form. This property could be beneficial for hemostatic dressing use, as it would allow for faster wound filling after implantation.[37]

Based on the theoretically reduced cross-link density and open pore structure in NTA−DEG foams, the dry mechanical property trends (decreased elastic modulus and tensile strength and increased ultimate elongation with NTA−DEG incorporation) were generally expected. Some of these differences could also be attributed to the reduced density of 30% NTA−DEG foams. The smaller differences in modulus and strength between NTA−DEG foams and controls in the wet state are again attributed to secondary intermolecular

https://doi.org/10.1021/acsabm.1c00516
ACS Appl. Bio Mater. XXXX, XXX, XXX−XXX

forces in the samples. The carbonyl linkages of the ester groups interact via secondary dipole interactions that are less affected by water in comparison with the hydrogen bonds between urethane linkages. Thus, plasticization does not affect the NTA−DEG foam flexibility to the same extent as that of control foams. While the wet mechanical properties are more similar between formulations, it may be beneficial to tune the stiffness of NTA−DEG foams in future studies by increasing HPED content or decreasing diisocyanate monomer chain length with butane diisocyanate in place of HDI.

4.2. Biological Characterization. All of the foams retained high cytocompatibility (>75%) over 72 h, which meets the ISO 10993 standard for cytocompatibility.[38] Future studies will focus on measuring cytocompatibility of degradation products and in vivo host response during degradation to provide a better understanding of the material biocompatibility. The absorbed blood amounts generally correlate with swelling ratios in water, with the control foam having the highest volume of absorbed blood and 15% NTA−DEG having the lowest volume. The decrease in blood absorption in the 30% NTA−DEG foam relative to the control foam could be attributed to the open pore structure, which likely reduced the amount of retained (anticoagulated) blood after removal.

Clotting times were measured relative to gauze. SMP foams all had slower clotting times with increased free RBCs at 0 and 6 min. However, by 12 min, all samples had fully clotted with no differences between free RBC levels. In general, the 30% NTA−DEG foam appeared to clot the slowest of the tested formulations. This trend was also seen in the platelet attachment numbers, where gauze had the highest number of platelets, followed by the control foam. The NTA−DEG foams had the lowest platelet numbers. The platelet images correlate with these results based on evidence of more advanced thrombus formation on the gauze sample. All SMP formulations promoted platelet attachment and activation, demonstrated by the protrusions on individual platelets. Control and 15% NTA−DEG foams had areas with platelet aggregates, a precursor to thrombus formation. The 30% NTA−DEG foams had the lowest levels of imaged platelet numbers and aggregates.

Interestingly, in our preliminary in vivo experiments in a porcine liver injury,[39] treatment with control foams slightly reduced blood loss and significantly increased animal survival in comparison with gauze treatment. Thus, based upon comparisons between gauze and control SMP foams, the in vivo clotting process is more complex than we are able to replicate with these initial in vitro studies and likely requires further investigation in less static conditions. However, it does appear that the modification with degradable NTA−DEG reduces the clotting capabilities of SMP foams. One of the main benefits of the SMP foam system is its synthetic tunability. We have parallel work that involves incorporation of antimicrobial phenolic acids into SMP foams to reduce infection risks.[40] In addition to their antimicrobial properties, phenolic acids demonstrate procoagulant activity.[41,42] Future work will focus on incorporating procoagulant species, such as phenolic acids, into the NTA−DEG foams to increase their clotting capabilities while maintaining the desired degradation profiles, open pore structures, and flexible mechanical properties.

4.3. Degradation Profiles. Control SMP foams have excellent hydrolytic stability. Despite the incorporation of hydrolytically labile ester linkages in NTA−DEG foams, they were very stable in accelerated hydrolytic degradation media after an initial drop in mass by ∼20% at the first time point. We hypothesize that this stability could be due to (i) relative hydrophobicity around the ester linkages to reduce water penetration into the network and (ii) initial degradation of only ester linkages and loss of NTA from the polymer, after which the remainder of the network was stable in 0.1 M NaOH. Based on prior studies showing that control foams degrade via oxidation of tertiary amines in HPED and TEA monomers, we hypothesized that NTA−DEG foams may degrade more quickly in oxidative conditions.[19,23] As the network degrades oxidatively, it becomes more hydrophilic, enabling increased water access to the hydrolytically degradable ester linkages to promote hydrolysis. Thus, degradation characterization was focused on samples in oxidative media (3% H_2O_2). Control foams had an initially slow degradation rate with an apparent increase in the rate at ∼42 days. The change in degradation rate of control foams is consistent with previous SMP foam degradation studies and corresponds with the observed erosion profile.[19,23] This result could be attributed to the relative brittleness of control foams (higher elastic modulus) that causes bulk erosion upon exposure to external forces during the characterization process. Namely, the foams are washed, dried, and weighed every 3−7 days. Increased brittleness can cause samples to break apart over time of repeated external force application. The nonlinear mass loss rates and differences in erosion profiles would likely affect tissue regeneration and load transfer in vivo as well and make estimation of in vivo degradation rates more complex.[43−45]

The NTA−DEG monomer was designed to provide multiple potential degradation points. NTA contains a tertiary amine similar to HPED and TEA, which has been previously shown to break down into carboxylic acid and ammonia byproducts.[46] The carboxylic acid groups locally decrease pH within the scaffold, which can accelerate hydrolysis of the ester linkages between NTA and DEG. Finally, DEG contains ether linkages, which (i) enhance hydrophilicity adjacent to the ester linkage to increase water access and (ii) may also degrade oxidatively. Ether oxidation produces carboxylic acids, alcohols, and aldehydes, and the carboxylic acids can further catalyze ester hydrolysis.[15] During the ether degradation process, there is a possibility that the carbon radicals can cross-link with each other to form cross-links. While cross-linking was not visible on the FTIR spectra (would be indicated by branched ether peak at ∼1172 cm^{-1}), it is possible that ether cross-linking occurred simultaneously to oxidative and hydrolytic degradation in 15% NTA−DEG foams to provide a more linear degradation profile and reduce bulk erosion.

The degradation rate of NTA−DEG foams can be easily tuned with variations in the NTA−DEG content. We hypothesize that degradation rates could be further controlled with other monomer variables, such as diisocyanate length, monomer hydrophobicity, and polyol functionality. These foams have linear in vitro mass loss rates that, if replicated in vivo, could be highly beneficial for graded load transfer from scaffolds to tissues during healing, particularly when considering the highly interconnected pores. While the focus of the current work is on hemorrhage control, these foams provide a potential platform for tissue engineering scaffolds in future work.

https://doi.org/10.1021/acsabm.1c00516
ACS Appl. Bio Mater. XXXX, XXX, XXX−XXX

5. CONCLUSIONS

This study reveals that incorporation of ester linkages using the new NTA−DEG monomer can increase the degradation rate of polyurethane SMP foams to clinically relevant time frames of 4−8 weeks[24] while maintaining desired thermal properties. Namely, a dry T_g above 40 °C ensures that the foams can be stored in their secondary shape, and a wet T_g below body temperature enables expansion to the primary shape after implantation. The new monomer also imparted other potentially valuable foam properties, including interconnects between the pores that may aid in tissue regeneration, very rapid volume recovery within 30 s to aid in hemostatic dressing delivery, and increased flexibility to potentially reduce tears or premature breakdown of scaffolds during delivery or healing. Incorporation of NTA−DEG reduced the clotting capabilities of SMP foams; thus, future studies with these foams will include incorporation of procoagulant species into the tunable material system. Beyond hemorrhage control, these foams provide a platform for future development into other regenerative medicine applications where scaffold degradation is desired.

■ ASSOCIATED CONTENT

Supporting Information

The Supporting Information is available free of charge at https://pubs.acs.org/doi/10.1021/acsabm.1c00516.

FTIR and 1H NMR spectrum of the synthesized NTA−DEG ester; representative images of lysates from clotting assay; glass transition temperatures and erosion profile of samples throughout degradation in 0.1 M NaOH; SEM micrographs for samples throughout degradation in 0.1 M NaOH; FTIR spectra of samples throughout degradation in 0.1 M NaOH; and FTIR spectra of dry samples and water interactions with polyurethane foams (PDF)

■ AUTHOR INFORMATION

Corresponding Author

Mary Beth B. Monroe − *Department of Biomedical and Chemical Engineering, Syracuse Biomaterials Institute, and BioInspired Syracuse: Institute for Material and Living Systems, Syracuse University, Syracuse, New York 13244, United States;* orcid.org/0000-0003-4540-5303; Phone: +1 (315)443-3323; Email: mbmonroe@syr.edu

Authors

Anand Utpal Vakil − *Department of Biomedical and Chemical Engineering, Syracuse Biomaterials Institute, and BioInspired Syracuse: Institute for Material and Living Systems, Syracuse University, Syracuse, New York 13244, United States;* orcid.org/0000-0002-6303-8562

Natalie Marie Petryk − *Department of Biomedical and Chemical Engineering, Syracuse Biomaterials Institute, and BioInspired Syracuse: Institute for Material and Living Systems, Syracuse University, Syracuse, New York 13244, United States*

Ellen Shepherd − *Department of Biomedical and Chemical Engineering, Syracuse Biomaterials Institute, and BioInspired Syracuse: Institute for Material and Living Systems, Syracuse University, Syracuse, New York 13244, United States*

Henry T. Beaman − *Department of Biomedical and Chemical Engineering, Syracuse Biomaterials Institute, and BioInspired Syracuse: Institute for Material and Living Systems, Syracuse University, Syracuse, New York 13244, United States*

Priya S. Ganesh − *Department of Biomedical and Chemical Engineering, Syracuse Biomaterials Institute, and BioInspired Syracuse: Institute for Material and Living Systems, Syracuse University, Syracuse, New York 13244, United States*

Katheryn S. Dong − *Department of Biomedical and Chemical Engineering, Syracuse Biomaterials Institute, and BioInspired Syracuse: Institute for Material and Living Systems, Syracuse University, Syracuse, New York 13244, United States*

Complete contact information is available at: https://pubs.acs.org/10.1021/acsabm.1c00516

Author Contributions

The manuscript was written through contributions of all authors. All authors have given approval to the final version of the manuscript.

Funding

This material is based on research sponsored by the U.S. Air Force under agreement number FA8650-18-2-6978. The U.S. Government is authorized to reproduce and distribute reprints for Governmental purposes notwithstanding any copyright notation thereon. The views and conclusions contained herein are those of the authors and should not be interpreted as necessarily representing the official policies or endorsements, either expressed or implied, of the U.S. Air Force or the U.S. Government.

Notes

The authors declare no competing financial interest.

■ REFERENCES

(1) Holcomb, J.; Caruso, J.; McMullin, N.; Wade, C. E.; Pearse, L.; Oetjen-Gerdes, L.; Champion, H. R.; Lawnick, M.; Farr, W.; Rodriguez, S.; Butler, F. Causes of Death in US Special Operations Forces in the Global War on Terrorism: 2001-2004. *US. Army Med. Dep. J.* **2007**, 24−37.

(2) Eastridge, B. J.; Mabry, R. L.; Seguin, P.; Cantrell, J.; Tops, T.; Uribe, P.; Mallett, O.; Zubko, T.; Oetjen-Gerdes, L.; Rasmussen, T. E.; Butler, F. K.; Kotwal, R. S.; Holcomb, J. B.; Wade, C.; Champion, H.; Lawnick, M.; Moores, L.; Blackbourne, L. H. Death on the Battlefield (2001-2011): Implications for the Future of Combat Casualty Care. *J. Trauma Acute Care Surg.* **2012**, *73*, S431−7.

(3) Alam, H. B.; Burris, D.; DaCorta, J. A.; Rhee, P. Hemorrhage Control in the Battlefield: Role of New Hemostatic Agents. *Mil. Med.* **2005**, *170*, 63−69.

(4) Dayan, L.; Zinmann, C.; Stahl, S.; Norman, D. Complications Associated with Prolonged Tourniquet Application on the Battlefield. *Mil. Med.* **2008**, *173*, 63−66.

(5) Navein, J.; Coupland, R.; Dunn, R. The Tourniquet Controversy. *J. Trauma Acute Care Surg.* **2003**, *54*, S219−S220.

(6) Sims, K.; Montgomery, H. R.; Dituro, P.; Kheirabadi, B. S.; Butler, F. K. *Management of External Hemorrhage in Tactical Combat Casualty Care: The Adjunctive Use of XStat™ Compressed Hemostatic Sponges: TCCC Guidelines Change 15-03*; 2016; Vol. *16*.

(7) Mueller, G. R.; Pineda, T. J.; Xie, H. X.; Teach, J. S.; Barofsky, A. D.; Schmid, J. R.; Gregory, K. W. A Novel Sponge-Based Wound Stasis Dressing to Treat Lethal Noncompressible Hemorrhage. *J. Trauma Acute Care Surg.* **2012**, *73*, S134.

(8) Kragh, J. F., Jr.; Aden, J. K.; Steinbaugh, J.; Bullard, M.; Dubick, M. A. Gauze vs XSTAT in Wound Packing for Hemorrhage Control. *Am. J. Emerg. Med.* **2015**, *33*, 974−976.

(9) He, J. M.; Wu, Y. D.; Wang, W.; Cheng, W. L.; Huang, Y. D.; Fu, B. Hemostatic, Antibacterial and Degradable Performance of the Water-Soluble Chitosan-Coated Oxidized Regenerated Cellulose Gauze. *Fibers Polym.* **2014**, *15*, 504−509.

(10) Dai, C.; Yuan, Y.; Liu, C.; Wei, J.; Hong, H.; Li, X.; Pan, X. Degradable, Antibacterial Silver Exchanged Mesoporous Silica Spheres for Hemorrhage Control. *Biomaterials* **2009**, *30*, 5364−5375.
(11) Ratner, B. D. A Pore Way to Heal and Regenerate: 21st Century Thinking on Biocompatibility. *Regen. Biomater.* **2016**, *3*, 107−110.
(12) Li, J.; Wu, X.; Wu, Y.; Tang, Z.; Sun, X.; Pan, M.; Chen, Y.; Li, J.; Xiao, R.; Wang, Z.; Liu, H. Porous Chitosan Microspheres for Application as Quick in Vitro and in Vivo Hemostat. *Mater. Sci. Eng. C* **2017**, *77*, 411−419.
(13) Monroe, M. B. B.; Easley, A. D.; Grant, K.; Fletcher, G. K.; Boyer, C.; Maitland, D. J. Multifunctional Shape Memory Polymer Foams with Bio-Inspired Antimicrobials. *ChemPhysChem* **2018**, *19*, 1999−2008.
(14) Behl, M.; Lendlein, A. Actively Moving Polymers. *Soft Matter* **2007**, *3*, 58−67.
(15) Christenson, E. M.; Anderson, J. M.; Hiltner, A. Biodegradation Mechanisms of Polyurethane Elastomers. *Corros. Eng. Sci. Technol.* **2007**, *42*, 312−323.
(16) Laschke, M. W.; Strohe, A.; Scheuer, C.; Eglin, D.; Verrier, S.; Alini, M.; Pohlemann, T.; Menger, M. D. In Vivo Biocompatibility and Vascularization of Biodegradable Porous Polyurethane Scaffolds for Tissue Engineering. *Acta Biomater.* **2009**, *5*, 1991−2001.
(17) Pretsch, T.; Jakob, I.; Müller, W. Hydrolytic Degradation and Functional Stability of a Segmented Shape Memory Poly(Ester Urethane). *Polym. Degrad. Stab.* **2009**, *94*, 61−73.
(18) Swan, K. G.; Swan, R. C. Principles of Ballistics Applicable to the Treatment of Gunshot Wounds. *Surg. Clin. North Am.* **1991**, *71*, 221−239.
(19) Weems, A. C.; Wacker, K. T.; Carrow, J. K.; Boyle, A. J.; Maitland, D. J. Shape Memory Polyurethanes with Oxidation-Induced Degradation: In Vivo and In Vitro Correlations for Endovascular Material Applications. *Acta Biomater.* **2017**, *59*, 33−44.
(20) Singhal, P.; Small, W.; Cosgriff-Hernandez, E.; Maitland, D. J.; Wilson, T. S. Low Density Biodegradable Shape Memory Polyurethane Foams for Embolic Biomedical Applications. *Acta Biomater.* **2014**, *10*, 67−76.
(21) Fan, X.; Chung, J. Y.; Lim, Y. X.; Li, Z.; Loh, X. J. Review of Adaptive Programmable Materials and Their Bioapplications. In *ACS Applied Materials and Interfaces*; American Chemical Society, 2016; pp 33351−33370.
(22) Weems, A. C.; Easley, A.; Roach, S. R.; Maitland, D. J. Highly Cross-Linked Shape Memory Polymers with Tunable Oxidative and Hydrolytic Degradation Rates and Selected Products Based on Succinic Acid. *ACS Appl. Bio. Mater.* **2019**, *2*, 454−463.
(23) Jang, L. K.; Fletcher, G. K.; Monroe, M. B. B.; Maitland, D. J. Biodegradable Shape Memory Polymer Foams with Appropriate Thermal Properties for Hemostatic Applications. *J. Biomed. Mater. Res. A* **2019**, *108*, 1281−1294.
(24) Jaganjac, E. T.; Kuba, T.; Visna, P.; Beitl, E.; Kalvach, J. Treatment of Gunshot Wounds and Prevention of Complications during the Healing Process. *Rozhl. Chir.* **2007**, *86*, 188−193.
(25) Nishikawa, M.; Hashida, M.; Takakura, Y. Catalase Delivery for Inhibiting ROS-Mediated Tissue Injury and Tumor Metastasis. *Adv. Drug Deliv. Rev.* **2009**, *61*, 319−326.
(26) Bryan, N.; Ahswin, H.; Smart, N.; Bayon, Y.; Wohlert, S.; Hunt, J. A. Reactive Oxygen Species (ROS) - a Family of Fate Deciding Molecules Pivotal in Constructive Inflammation and Wound Healing. *Eur. Cells Mater.* **2012**, *24*, 249−265.
(27) Bandzierz, K.; Reuvekamp, L.; Dryzek, J.; Dierkes, W.; Blume, A.; Bielinski, D. Influence of Network Structure on Glass Transition Temperature of Elastomers. *Materials* **2016**, *9*, 607.
(28) Fox, T. G.; Loshaek, S. Influence of Molecular Weight and Degree of Crosslinking on the Specific Volume and Glass Temperature of Polymers. *J. Polym. Sci.* **1955**, *15*, 371−390.
(29) Laycock, B.; Nikolić, M.; Colwell, J. M.; Gauthier, E.; Halley, P.; Bottle, S.; George, G. Lifetime Prediction of Biodegradable Polymers. *Prog. Polym. Sci. Sci.* **2017**, *71*, 144−189.
(30) Dunnill, C.; Patton, T.; Brennan, J.; Barrett, J.; Dryden, M.; Cooke, J.; Leaper, D.; Georgopoulos, N. T. Reactive Oxygen Species (ROS) and Wound Healing: The Functional Role of ROS and Emerging ROS-Modulating Technologies for Augmentation of the Healing Process. *Int. Wound J.* **2017**, *14*, 89−96.
(31) Rodriguez, J. N.; Miller, M. W.; Boyle, A.; Horn, J.; Yang, C. K.; Wilson, T. S.; Ortega, J. M.; Small, W.; Nash, L.; Skoog, H.; Maitland, D. J. Reticulation of Low Density Shape Memory Polymer Foam with an in Vivo Demonstration of Vascular Occlusion. *J. Mech. Behav. Biomed. Mater.* **2014**, *40*, 102−114.
(32) Nash, L. D.; Docherty, N. C.; Monroe, M. B. B.; Ezell, K. P.; Carrow, J. K.; Hasan, S. M.; Gaharwar, A. K.; Maitland, D. J. Cold Plasma Reticulation of Shape Memory Embolic Tissue Scaffolds. *Macromol. Rapid Commun.* **2016**, *37*, 1945−1951.
(33) Walthers, C. M.; Nazemi, A. K.; Patel, S. L.; Wu, B. M.; Dunn, J. C. Y. The Effect of Scaffold Macroporosity on Angiogenesis and Cell Survival in Tissue-Engineered Smooth Muscle. *Biomaterials* **2014**, *35*, 5129−5137.
(34) Xiao, X.; Wang, W.; Liu, D.; Zhang, H.; Gao, P.; Geng, L.; Yuan, Y.; Lu, J.; Wang, Z. The Promotion of Angiogenesis Induced by Three-Dimensional Porous Beta-Tricalcium Phosphate Scaffold with Different Interconnection Sizes via Activation of PI3K/Akt Pathways. *Sci. Rep.* **2015**, *5*, No. 9409.
(35) Lendlein, A.; Kelch, S. Shape-Memory Polymers. *Angew. Chem., Int. Ed.* **2002**, *41*, 2034−2057.
(36) Yu, Y.-J.; Hearon, K.; Wilson, T. S.; Maitland, D. J. The Effect of Moisture Absorption on the Physical Properties of Polyurethane Shape Memory Polymer Foams. *Smart Mater. Struct.* **2011**, *20*, No. 085010.
(37) Vyas, K. S.; Saha, S. P. Comparison of Hemostatic Agents Used in Vascular Surgery. *Expert Opin. Biol. Ther.* **2013**, *13*, 1663−1672.
(38) ISO, P. *Biological Evaluation of Medical Devices—Part 5: Tests for in Vitro Cytotoxicity*; International Organization for Standardization: Geneva, 2009; p 34.
(39) Beaman, H. T.; Shepherd, E.; Satalin, J.; Blair, S.; Ramcharran, H.; Serinelli, S.; Gitto, L.; Dong, K. S.; Nieman, G.; Schauer, S. G.; Monroe, M. B. B. Hemostatic Shape Memory Polymer Foams With Improved Survival in a Lethal Traumatic Hemorrhage Model. *SSRN Electron. J.* **2021**, 1.
(40) Monroe, M. B. B.; Easley, A. D.; Grant, K.; Fletcher, G. K.; Boyer, C.; Maitland, D. J. Multifunctional Shape-Memory Polymer Foams with Bio-Inspired Antimicrobials. *ChemPhysChem* **2018**, *19*, 1999−2008.
(41) Huang, L.; Lin, C.; Li, A.; Wei, B.; Teng, J.; Li, L. Pro-Coagulant Activity of Phenolic Acids Isolated from Blumea Riparia. *Nat. Prod. Commun.* **2010**, *5*, No. 1934578X1000500.
(42) Liu, J.; Du, C.; Beaman, H. T.; Monroe, M. B. B. Characterization of Phenolic Acid Antimicrobial and Antioxidant Structure−Property Relationships. *Pharmaceutics* **2020**, *12*, No. 419.
(43) Lloyd, A. W. Interfacial Bioengineering to Enhance Surface Biocompatibility. *Med. Device Technol.* **2002**, *13*, 18−21.
(44) Nair, L. S.; Laurencin, C. T. Biodegradable Polymers as Biomaterials. *Prog. Polym. Sci.* **2007**, *32*, 762−798.
(45) Song, R.; Murphy, M.; Li, C.; Ting, K.; Soo, C.; Zheng, Z. Current Development of Biodegradable Polymeric Materials for Biomedical Applications. *Drug Des. Devel. Ther.* **2018**, *12*, 3117.
(46) Boyle, A. J.; Wierzbicki, M. A.; Herting, S.; Weems, A. C.; Nathan, A.; Hwang, W.; Maitland, D. J. In Vitro Performance of a Shape Memory Polymer Foam-Coated Coil Embolization Device. *Med. Eng. Phys.* **2017**, *49*, 56−62.

ChemPubSoc Europe

DOI: 10.1002/cphc.201701015

CHEMPHYSCHEM Articles

Special Issue

Multifunctional Shape-Memory Polymer Foams with Bio-inspired Antimicrobials

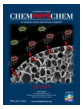

Mary Beth Browning Monroe,* Alexandra D. Easley, Katie Grant, Grace K. Fletcher, Calla Boyer, and Duncan J. Maitland[a]

Despite a number of clinically available hemostats, uncontrolled bleeding is the primary cause of trauma-related death. Shape-memory polymer (SMP) foams have a number of desirable properties for use as hemostats, including shape recovery to enable delivery into bleed sites, biocompatibility, and rapid blood clotting. To expand upon this material system, the current work aims to incorporate phenolic acids, which are honey-based antimicrobial agents, into SMP foams. We showed that cinnamic acid (CA) can be utilized as a monomer in SMP synthesis to provide foams with comparable pore structure and retained cytocompatibility. The addition of CA enabled tuning of thermal and shape-memory properties within clinically relevant ranges. Furthermore, the modified foams demonstrated initial and sustained antimicrobial effects against gram-positive and gram-negative bacteria. These multifunctional scaffolds demonstrate potential for use as hemostats to improve upon current hemorrhage treatments and provide a new tool in tuning the biological and material properties of SMP foams.

1. Introduction

Hemorrhage is the leading cause of potentially preventable death on the battlefield.[1] The current standard of field care is to utilize gauze in combination with tourniquets; however, these treatments are insufficient for up to 80% of wounds.[2] Furthermore, tourniquets only serve as temporary measures against blood loss, as tourniquet use beyond approximately 4–6 h is associated with limb damage and loss.[3] An improved hemostat material could enable earlier tourniquet removal before patients can receive treatment at a fixed facility.

Newly developed treatments seek to replace gauze by filling wounds with hemostatic materials to provide stable clots with reduced tourniquet use. Of these materials, such as fibrin, oxidized cellulose, or chitosan,[4] few have sufficiently proven their value on the battlefield. A particularly promising new hemostat is XStat™ (RevMedx, Inc., Wilsonville, OR), which has improved time to hemostasis, ease of application, and survival rates compared to conventional hemostats.[5] XStat™ was first used on the field in May 2016 with promising results. The XStat™ device is an applicator filled with small, compressed cellulose sponges that rapidly expand to fill and apply pressure to deep, non-compressible wounds. Despite the numerous advantages of the XStat™ technology, the insertion of 92 miniature sponges into an open wound results in a 22-fold increase in device removal time compared to conventional gauze due to the need to remove each individual sponge from the wound bed.[6] Additionally, these sponges must be removed from the patient within 4 h, limiting their applicability in prolonged field care applications where device removal within 4 h may not be possible. The current standard of care on the battlefield involves the use of a broad spectrum antibiotic regimen in combination with frequent dressing changes to prevent bacterial and fungal infections; however, rising concerns over antibiotic resistance requires the use of alternative treatment methods, and dressing changes are not always feasible during battle.[7]

In addition to clinically-available hemostats, a number of research groups are developing new hemostatic materials to address this large clinical need. For example, Wong et al. recently reported on a biodegradable, radiopaque, poly(ethylene glycol) (PEG)/poly(dl-lactide-*co*-glycolide) (PLGA) composite material that cuts of vascular blood flow by a swelling-induced shape-memory effect.[8] This device cut off blood flow in various arteries in a rabbit model within 2 min. Further characterization of the material thrombogenicity and stability over time is required, and it is unclear how scalable the shape recovery profiles are within a larger bleeding wound or how effective the material would be at reducing wound infection risks. However, this technology shows promise for use in embolic applications. Another recently developed hydrogel-based hemostatic material includes an injectable nanofibrous peptide hydrogel that has been loaded with snake-venom derived Batroxobin.[9] The material promotes clotting by physically blocking blood flow and utilizing a hemostatic drug, even in the presence of heparin, resulting in improved liver incision hemostasis in a rat model in comparison to clinical controls. While this technology could be useful, particularly for patients undergoing anticoagulant therapies, the time and cost to translate a combination

[a] *Dr. M. B. B. Monroe, A. D. Easley, K. Grant, G. K. Fletcher, C. Boyer, Dr. D. J. Maitland*
Department of Biomedical Engineering
Texas A&M University
5045 Emerging Technologies Building
3120 TAMU, College Station, TX 77843-3120 (USA)
E-mail: mbbmonroe@tamu.edu

Special Issue An invited contribution to a Special Issue on Smart Materials

device (biologic/scaffold and drug) limits its clinical feasibility. An easily translatable technique that was recently reported upon involves the use of hydrophobically-modified chitosan (hm-C) gauze.[10] hm-C has improved hemostatic capabilities in comparison to unmodified chitosan and outperformed chitosan in a lethal porcine bleed model; however, no statistical differences were found in key endpoint data, and this technology does not address the potential for wound infections. Thus, more research is required to determine if hm-C provides the needed improvements in hemostatic wound care. One recent approach to infection control involves a layer-by-layer assembled polymeric scaffold with controlled thrombin (to promote clotting) and vancomycin (to prevent infection) release.[11] While these scaffolds show blood clotting and antimicrobial efficacy, their film geometry prevents delivery to irregularly-shaped wounds, and the use of vancomycin limits efficacy against modified drug-resistant organisms. These recent research efforts highlight the difficulties in addressing this significant clinical problem.

Shape-memory polymer (SMP) foams provide a biomaterial platform with numerous potential benefits for use as hemostatic dressings to overcome current treatment limitations. Thermal SMPs are 'smart' materials that are fabricated in a permanent, primary shape and subsequently heated about a transition temperature, deformed, and cooled to lock in a secondary shape. This secondary shape is retained until application of a thermal stimulus, upon which the primary shape is recovered.[12] SMP foams can be synthesized, in which the primary shape is an expanded, open porous foam and the secondary shape is a compressed scaffold. Cold hibernated elastic memory (CHEM) foams were one of the first SMP foam compositions studied for use in biomedical applications, due to the ability of cells to infiltrate the porous scaffolds to promote healing.[13] Previously, Ellson et al. fabricated thiol-epoxy SMP foams with high shape recovery.[14] This work demonstrated the using of foaming variables to tune mechanical properties independently of material chemistry, one of the many benefits of a porous SMP system. Zhang et al. reported on a bioactive SMP foam wherein the shape-memory properties are utilized to shape-fill irregular bone defects.[15] Our group has developed a polyurethane SMP foam system for embolic applications.[16] The foam system can be designed to actuate in aqueous conditions between 15 and 45 °C (ca. 40–70 °C in dry conditions), and actuation times can be tuned between 30 s and 30 min. SMP foams demonstrated excellent biocompatibility over 90 and 180 days of implantation in a porcine aneurysm model.[17] Most importantly for the proposed application, these foams induce rapid clotting due to their high surface area and thrombogenic material chemistry; in a porcine hind limb vessel, SMP foams promoted arterial hemostasis within 90 s of device deployment.[18] SMP foams have minimal particulate generation, and no undesired downstream clotting has been observed in prior in vivo occlusion studies.[17–19] We previously modified SMP foams with a hydrogel filler to enable increased water/blood absorption with a methodology that could be applied to any SMP foam chemistry.[20] This material system enables application of a compressed device in a deep, irregularly-shaped bleed site, which would rapidly expand upon heating to body temperature to space-fill the wound volume and promote hemostasis.

One of the primary benefits of the SMP system is its tunable material chemistry. For example, previous work has incorporated degradable linkages and radiopaque monomers into the SMP backbone.[21] To enhance hemostatic device performance, antimicrobial agents can be introduced into the polymer network. Incorporated antimicrobials could work in conjunction with oral antibiotics to reduce infection risks and the need for frequent dressing changes.[22] To address concerns about antibiotic-resistant bacterial strains, antimicrobial phenolic acids were utilized in the current study to provide a non-drug approach.[23] Bees produce plant-derived phenolic acids in their honey, which protect hives against microbes and viruses. Phenolic acids exhibit broad antimicrobial properties, and have been shown to be effective against multi-drug resistant organisms (MDROs).[24] For example, antibiotic-resistant bacteria that were obtained from hospitals (*Enterobacter aerogenes*, *Escherichia coli*, and *Staphylococcus aureus)* were susceptible to cinnamic acid.[24c] A recent review covers the efficacy of a number of phenolic acids, including cinnamic, gentisic, and benzoic acids, against *Candida* infections (planktonic and biofilms, drug susceptible and drug resistant).[25]

Here, we developed the methodology to incorporate native and modified cinnamic acid (CA) into the SMP system, Figure 1. The resulting scaffolds were characterized to ensure that the desirable SMP properties were maintained, including density, pore size and structure, thermal properties, shape recovery profiles, and cytocompatibility. An emphasis was placed on design of a SMP foam hemostat that could be stored in extreme battlefield conditions and actuate quickly once exposed to water in blood at body temperature. Antimicrobial efficacy against *Escherichia coli* (*E.coli*) and *Staphylococcus epidermidis* (*Staph. epi.*) was characterized after soaking samples for up to 30 days in saline at body temperature to gain an understanding of initial and sustained antimicrobial effects.

2. Results and Discussion

2.1. Synthesis of CA and HCA-Containing SMPs

To enable its incorporation without sacrificing polyurethane network crosslink density, cinnamic acid (CA) was modified via esterification with N,N,N′,N′-tetrakis(2-hydroxypropyl) ethylenediamine (HPED) to form a CA-containing triol (HCA). Successful synthesis of HCA was confirmed via Fourier transform infrared (FTIR) and nuclear magnetic resonance (NMR) spectroscopy. In the FTIR spectra, a relative decrease in the hydroxyl groups can be observed at approximately 3350 cm^{-1}, and ester formation was confirmed via a shift in the carbonyl peak from approximately 1680 to 1710 cm^{-1}, Figure 2A. NMR showed the presence of esterified CA and HPED, with around 90% functionalization, Figure 2B.

Upon successful synthesis of HCA, SMP foams were prepared with 10, 20, and 30% HCA (mol% of hydroxyl groups, based off of 3 hydroxyl groups per mole of HCA). Qualitatively, the

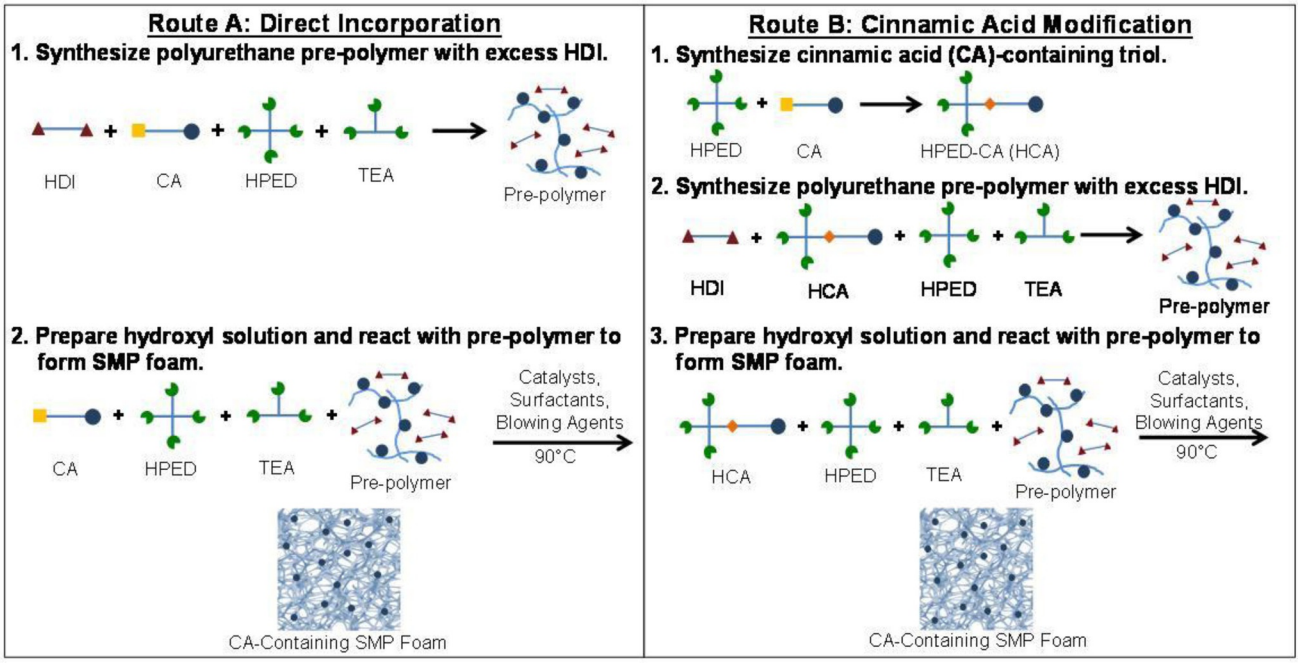

Figure 1. Schematic representation of CA incorporation into SMP foams. In route A, a pre-polymer was prepared with CA, hydroxypropyl ethylene diamine (HPED), triethanolamine (TEA), and excess hexamethylene diisocyanate (HDI). The pre-polymer was reacted with the remaining CA, HPED, and TEA in the presence of catalysts, surfactants, and blowing agents while heating to form a CA-containing SMP foam. In route B, the carboxylic acid group on CA was esterified with a hydroxyl group on HPED to form HCA. Then, HCA was used as a foaming monomer in place of CA in the same method utilized for Route A to form a CA-containing SMP foam.

foaming process went as expected, with no needed changes to the protocol relative to that of control foams. Additionally, foams were made with 10, 20 and 30% CA (mol% of hydroxyl groups, based off of 1 hydroxyl group (i.e. carboxylic acid) per mole of CA). The 10% CA foams rose as expected, but 20 and 30% CA foams did not form. This result was attributed to the termination of the polyurethane network upon reactions between HDI and mono-functional CA. At higher CA concentrations, a stable network was not able to form. While direct incorporation of CA is faster and simpler, its single functional group is a limitation to its effective use in this SMP system. This result also validates the additional HCA synthesis step, as it allows for more effective incorporation of higher concentrations of CA. The relatively straightforward synthesis method of HCA could be utilized with a range of phenolic acids or other carboxylic acid-containing functional molecules (e.g. drugs, bioactive factors) in future work to impart new properties to the SMP system. Phenolic acids have been esterified with other hydroxyl containing groups in previous work, further demonstrating the potential to expand upon the current work with other functional monomers.[24b, 26]

ATR-FTIR spectra were obtained of CA and HCA containing foams, Figure 2C. There is an additional peak at approximately 1615 cm^{-1} in all of the CA and HCA foams that is attributed to the C=C groups in the ring structure. The relative absorbance of this peak increases slightly (relative to the urethane peak at ca. 1680 cm^{-1}) with increased HCA concentration. In the 10% CA spectra, the relative absorbance at the 1615 cm^{-1} peak is between that of 20 and 30% HCA, indicating a higher incorporation efficiency with the unmodified CA. These spectra confirm successful incorporation of CA and HCA into the SMP network. Both routes are viable for effective synthesis of phenolic acid-containing foams.

2.2. Structural Properties

Foam density and pore sizes were assessed to verify the qualitative observations of successful foam blowing with CA and HCA, Figure 3. In general, CA and HCA-containing foams retain the ultralow density that is characteristic of this SMP system, Figure 3A.[27] The 10% HCA foams had a higher density, and there was a trend of decreasing density with increased HCA concentration. These results correspond with pore size measurements, with increasing pore sizes as HCA concentration is increased, Figure 3B. Qualitatively, 10 and 20% HCA foams have less rounded pores, which further correlates with density measurements, Figure 3C. Despite these minor differences, overall, CA and HCA foam pore sizes were comparable to those of the control foam, Figure 3B-**C**. Improved isotropicity (ratio between pore sizes in the axial and transverse foaming directions) was observed with the CA and HCA foams, indicating that the new monomers aided in constricting the foam rise process to provide more homogeneous pores, Figure 3B. It should be noted that the reaction between the carboxylic acid group on CA and isocyanates yields CO_2 to provide an additional chemical blowing agent in the 10% CA foam formulation; however, this variable did not significantly affect the foaming process or resulting foam morphology. Overall, these results show that CA and HCA can be incorporated into SMP foams with minimal protocol changes to provide structurally

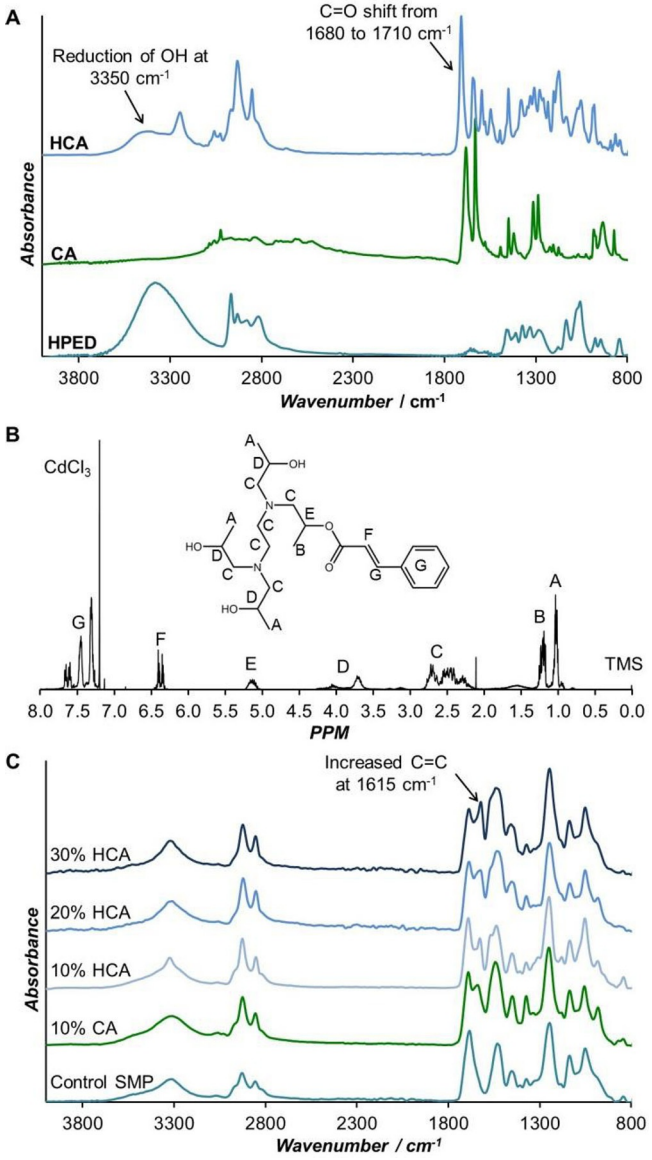

Figure 2. Spectral confirmation of synthesis of HCA/CA foams. A) Transmission FTIR spectra of HCA compared to HPED and CA; B) NMR spectra of HCA; C) attenuated total reflectance FTIR spectra of the control, CA, and HCA foams.

similar materials, further indicating the potential for this method to be used effectively with other functional monomers with similar reactive groups.

2.3. Thermal and Shape-Memory Properties

For effective field use, SMP foam-based hemostats must retain their compressed geometries at the high temperatures that are reached in desert climates (e.g. up to ca. 45 °C in Iraq) under dry storage conditions and then rapidly expand upon exposure to water in body temperature blood. As an initial indication of these capabilities, SMP foam glass transition temperatures (T_g values) were measured under dry and wet conditions, Figure 4A –B. The 10% CA foam dry T_g was similar to that of the control, and both were below the required 45 °C for field use. The stiff ring structure of CA is hypothesized to reduce backbone flexibility and increase T_g; however, incorporation of the monofunctional group is expected to reduce the overall crosslink density, which had an opposing effect on T_g.[28] The slightly broadened transition zone of the 10% CA foams (Figure 4B) is also attributed to the network irregularities that occurred with monofunctional CA incorporation. To increase dry T_g of CA foams to a useful level, overall crosslink density could be increased by utilizing more HPED, or backbone stiffness could be further increased with the introduction of stiffer monomers, such as trimethyl hexamethylene diisocyanate.[28a] Incorporation of HCA allowed for crosslink density to be retained while increasing backbone stiffness, resulting in increases in dry T_g with increased HCA content. All HCA-containing foams had dry T_g values at or above 45 °C. Our group previously showed that SMP foams that were aged in the compressed state for up to two years at room temperature or for 90 days at 55 °C (below dry T_g) had minimal changes in dimensions, wet and dry T_g, and volume recovery profiles.[29] While studies would need to be conducted on the current foam formulation to correlate these results, the high dry T_g of HCA-containing foams provides an initial indication of their potential for use on the battlefield without premature expansion. Additionally, HCA incorporation provides a new tool for tuning SMP foam thermal properties. All CA and HCA foams had wet T_g values below 30 °C, allowing for expansion after exposure to body temperature blood, even if the patient is in hypovolemic shock from blood loss and subjected to hypothermia.[30]

To further explore the functional capabilities of CA and HCA SMP foams, their volume expansion profiles were characterized in 37 °C water, Figure 4B --**C**. CA foams had more rapid expansion as compared to controls, which is attributed to their theoretically decreased crosslink density due to the incorporation of a monofunctional monomer. Increasing HCA content resulted in slower volume expansion, correlating with increased T_g measurements, and is attributed to increased foam hydrophobicity and backbone stiffness with the introduction of the ring structure in CA. The increase in expansion rate of 10 and 20% HCA foams relative to the control is likely due to network inconsistencies. Although high average functionalization of HCA was achieved, the synthesized monomer is a mix of HPED with varied numbers of tethered CA molecules. The resulting network inhomogeneity can result in more rapid volume expansion, despite increased hydrophobicity. This effect was outweighed with increased HCA content in the 30% HCA foam, where increased hydrophobicity likely had a larger effect on slowing down expansion than network inconsistencies. To address severe bleeds, SMP-based hemostats should achieve full expansion as quickly as possible. Full expansion of 10 and 20% HCA in less than 2 min in combination with their high dry T_g values is highly promising for their potential use as hemostats on the battlefield. The variations in volume expansion rates with increased HCA content further validates the ability to use HCA incorporation as a tool for tuning SMP foam properties.

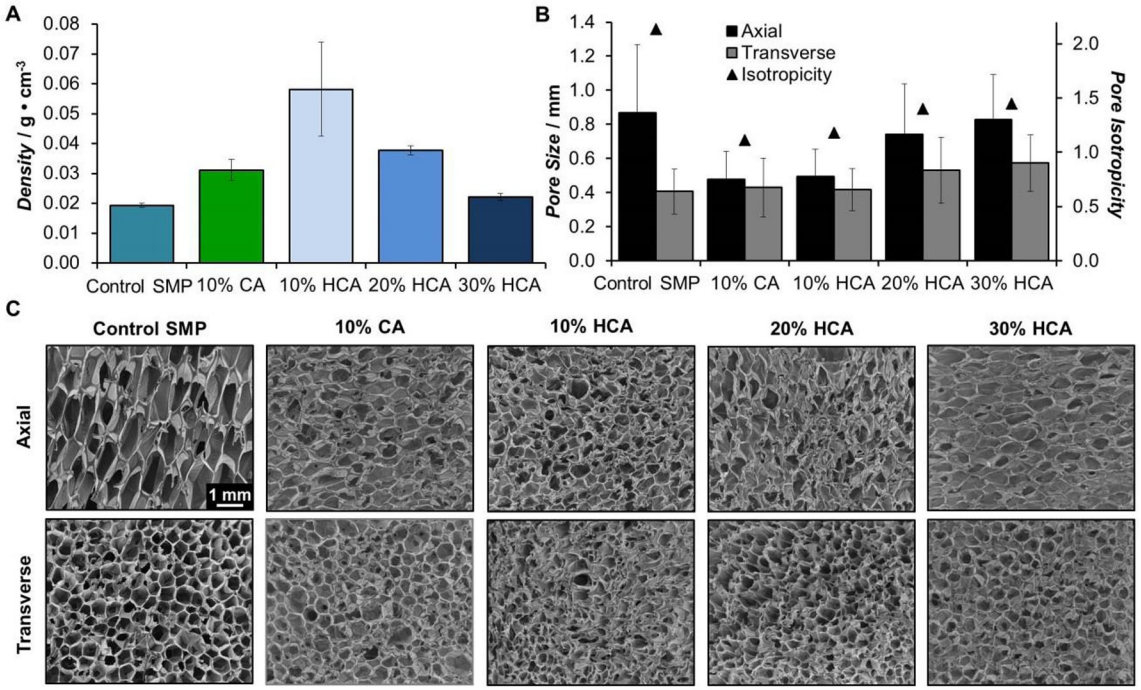

Figure 3. SMP foam structural properties. A) Density, B) pore size (axial and transverse foaming directions) and isotropicity (ratio between pore sizes in the axial and transverse foaming directions), and C) representative scanning electron microscopy images in the axial and transverse foaming directions. Scale bar applies to all images.

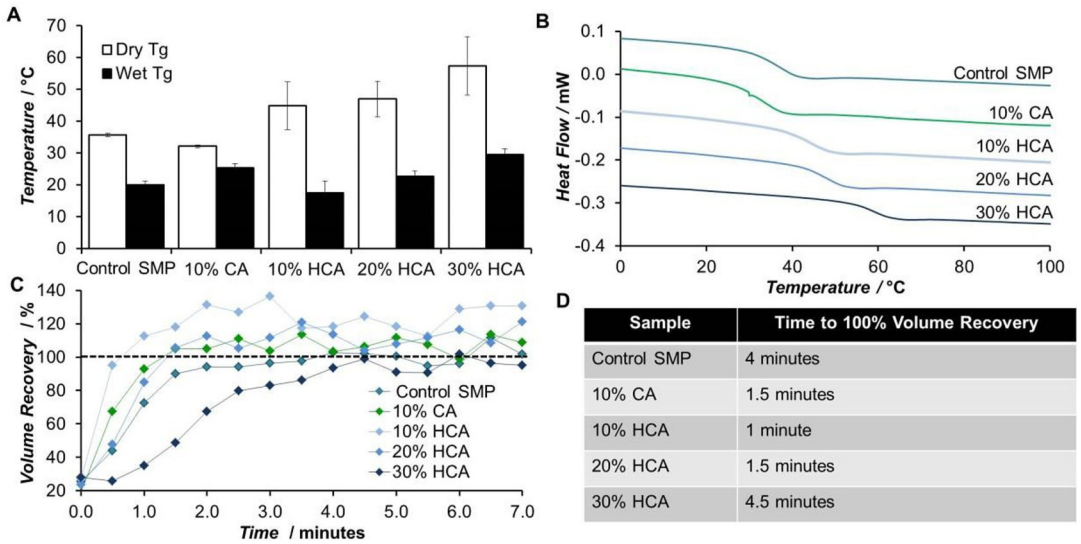

Sample	Time to 100% Volume Recovery
Control SMP	4 minutes
10% CA	1.5 minutes
10% HCA	1 minute
20% HCA	1.5 minutes
30% HCA	4.5 minutes

Figure 4. Thermal and shape-memory properties of HCA/CA foams. A) Dry and wet glass transition temperatures (T_g), B) differential scanning calorimetry thermograms utilized to determine dry T_g values (spectra have been shifted vertically to enable comparison), C) volume recovery profile in 37 °C water, and d) time to 100% volume recovery in 37 °C water.

2.4. Cytocompatibility

As an initial indication of CA and HCA-containing SMP cytocompatibility, human dermal fibroblasts (HDFs) were indirectly exposed to SMP films, and their morphology, initial attachment, and proliferation were qualitatively assessed, Figure 5. Initial attachment was similar between wells containing SMP films and the positive control, TCPS. HDFs were evenly attached across the well surfaces and well spread. The negative control, BSA-coated TCPS, had lower attachment and rounded cells. At 72 h, HDFs had elongated and proliferated in all SMP film-containing wells and the TCPS control with some areas of confluence. The BSA negative control wells still had low attachment numbers and lower spreading after 72 h. While further assessment is required to determine direct cell interactions with CA and HCA-containing SMP foams, these studies indicate

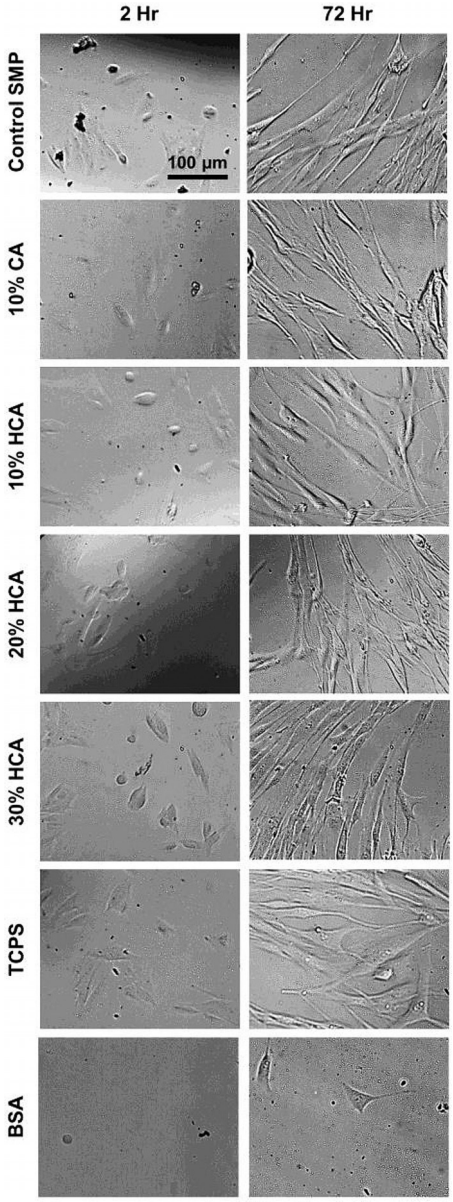

Figure 5. Representative bright-field images of human dermal fibroblasts after 2 and 72 h of contact with SMP films. Scale bar applies to all images.

that the modifications did not negatively affect the cytocompatibility of the base SMP formulation, which is promising for their use as biomaterial scaffolds.[17,31]

2.5. Antimicrobial Properties

To measure antimicrobial efficacy of CA and HCA following incorporation into SMPs, colony forming unit (CFU) density of *E. coli* (gram negative) and *Staph. epi.* (gram positive) were measured following exposure to SMP films. There were large reductions in *E. coli* CFUs after exposure to CA and HCA-containing films in comparison to unmodified control SMP films. CFU density was at or below that of drug-based (penicillin streptomycin, P/S) controls, Figure 6A. CFU reductions relative to unmodified control SMP films were significant for 10% CA and 30% HCA films. The improved performance of CA at lower concentrations is likely due to more effective incorporation, as indicated by an increased C=C peak at 1615 cm^{-1} in the FTIR spectra (Figure 2C). The increased efficacy of 30% HCA was expected, as antimicrobial properties should increase with increased CA concentration in the films.[24c] Similar results were observed with *Staph. epi*, with significant decreases in CFU density for 10% CA, 20% HCA, and 30% HCA films to levels at or below the drug-based (P/S) control, Figure 6B. There was a trend of decreasing CFU density with increased HCA concentration, as expected. In previous work, some phenolic acids have shown increased antimicrobial efficacy after esterification.[32] This result has not been observed with CA, and the comparable results between the CA and HCA systems were expected. However, future work will include incorporation of phenolic acids that benefit from esterification to assess whether further improvements can be made with antimicrobial SMPs. Overall, these results demonstrate that the antimicrobial properties of CA are retained following incorporation into SMPs with and without prior modification. The comparable efficacy to P/S is highly promising for potential use of CA or HCA-containing SMPs against drug resistant organisms. This data is backed up by previous work in which antibiotic-resistant bacteria that were obtained from hospitals (*Enterobacter aerogenes*, *Escherichia coli*, and *Staphylococcus aureus)* were susceptible to CA.[24c]

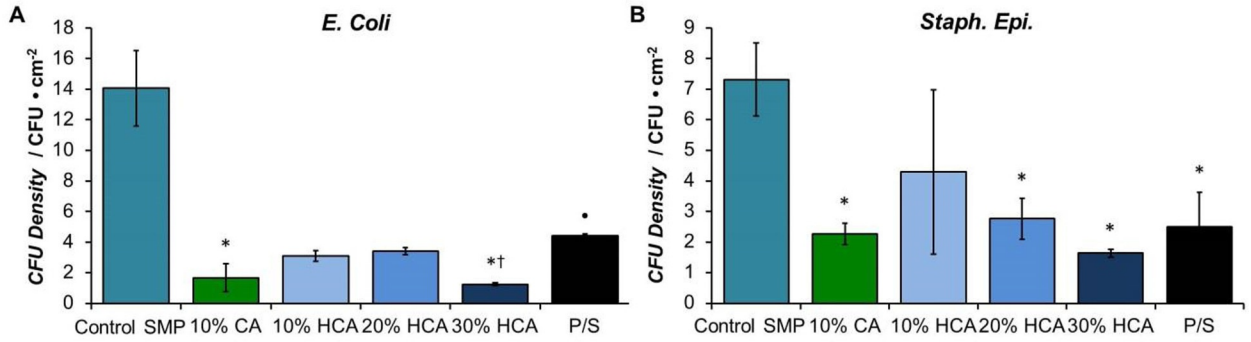

Figure 6. CFU density of A) *E. coli* and B) *Staph. epi.* after exposure to unmodified control, CA, HCA, and penicillin-streptomycin (P/S)-soaked control SMP films. *$p < 0.05$ relative to the control; †$p < 0.05$ relative to 10% HCA and 20% HCA; •$p < 0.05$ relative to all other samples.

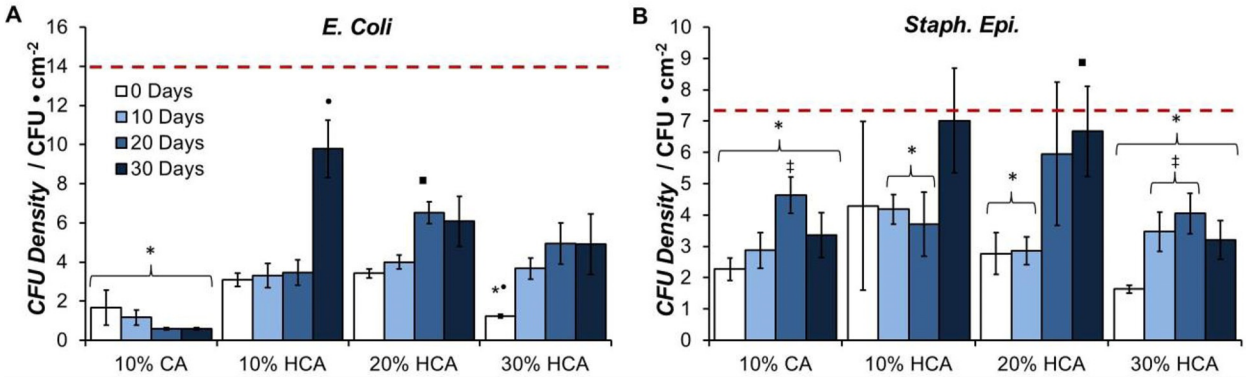

Figure 7. CFU density of A) *E. coli* and B) *Staph. epi.* after exposure to CA and HCA SMP films that had been soaked in phosphate buffered saline at 37 °C for up to 30 days. Red line: control CFU density. *$p < 0.05$ relative to the control; *$p < 0.05$ relative to all other time points within formulation; ■$p < 0.05$ relative to 10 and 20 day samples within formulation; ‡$p < 0.05$ relative to 0 day sample within formulation.

To characterize antimicrobial property retention, CA and HCA containing films were soaked in saline solution at 37 °C for up to 30 days, and *E. coli* and *Staph. epi.* CFU density was measured after exposure to soaked films. All 10% CA films retained significantly lower CFU density compared to the unmodified control SMP for both bacteria types, Figure 7. The formation of a urethane bond between CA and HDI in the SMP network provides a biostable linkage that is not susceptible to hydrolysis. Thus, we hypothesize that the majority of the CA was retained in the films throughout the soaking period, providing a sustained antimicrobial effect. The 10% HCA films had comparable CFU densities up to 20 days of soaking, with increases for the 30 day samples that approached the control film value (red dashed line) for both bacteria types. Since HCA is incorporated into the SMP network via an ester linkage, it is likely that hydrolysis caused HCA concentration reductions over time. A similar trend was observed with 20% HCA samples, with increases in the CFU density after exposure to the 20 and 30 day soaked films. Increases in *E. coli* density were lower for 20% HCA at 30 days than those for 10% HCA, indicating a higher retained HCA concentration with increased initial concentration. This trend was further confirmed with 30% HCA films. While CFU density increases were observed between the 0 and 10 day soaked samples, indicating an initial loss of HCA, the CFU density did not dramatically change past 10 days of soaking and never approached that of control films. Thus, even with the hydrolytically-labile linkage, HCA provides a sustained antimicrobial effect in SMPs when incorporated at higher concentrations. These results combined with the favorable thermal and shape-memory properties of HCA-containing SMPs indicate their potential for use as antimicrobial hemostats.

3. Conclusions

This work demonstrates successful incorporation of CA, a honey-based phenolic acid, into SMP foams via two routes. The resulting foams retain the desirable porous structure of the control SMP while providing tunable thermal transitions and shape recovery properties that are ideal for their use in hemostats for bleeding control. Namely, CA-based SMPs were designed with high dry T_g values to enable their storage under extreme battlefield conditions and low wet T_g values to enable their rapid shape recovery upon exposure to blood at body temperature. Furthermore, CA-based SMPs have high cytocompatibility while effectively reducing bacterial growth to levels that are comparable to penicillin/streptomycin-based treatments, even after 30 days of storage in saline at body temperature. Overall, this system shows promise for future use in a hemostat device that is easy-to-use, biocompatible, and antimicrobial. An additional benefit to phenolic acids is their antioxidant properties; phenolic acids contain hydrogen donating groups that scavenge free radicals and reduce oxidation.[33] Recently, we found that SMP foams are susceptible to oxidative degradation.[34] Thus, in future work, we will obtain oxidative degradation profiles of phenolic acid-containing SMP foams in addition to expanding the library of phenolic acids utilized in SMP foaming to further characterize their tunability.

Experimental Section

Materials

DC 198, DC 5943, BL-22, T-131, and Enovate were purchased from Evonik (Essen, Germany) and used as received. All other chemicals were purchased from Sigma–Aldrich Inc. (St. Louis, MO) and used as received.

Phenolic Acid Monomer Synthesis and Characterization

N,N,N′,N′-tetrakis(2-hydroxypropyl) ethylenediamine (HPED)-cinnamic acid (HCA) was synthesized using an esterification procedure. Cinnamic acid (CA, 1 molar eq.) was added to a round bottom flask and dissolved in chloroform. Then, 4-(dimethylamino) pyridine (DMAP, 0.1 molar eq.) was added to the flask and dissolved. HPED (1 molar eq.) was weighed out in a separate vial, dissolved in chloroform, and added dropwise to the reaction flask. The flask was placed on ice to cool for approximately 5 min. N,N′-dicyclohexyl carbodiimide (DCC, 1.1 molar eq.) was weighed into a separate vial, dissolved in chloroform, and added dropwise to the chilled reaction vessel. The reaction was stirred under nitrogen on ice for 5 min and then allowed to proceed at room temperature for 3 h. After the reaction was complete, the flask was placed at 0 °C for 30 min to precipitate dicyclohexyl urea, which was then removed via vacuum filtration. The reaction solution was washed

twice with 1 molar eq. of 0.1 M HCl and then washed with an aqueous saturated sodium bicarbonate solution. The organic phase was dried over magnesium sulfate and filtered. Then, chloroform was removed using rotary evaporation following drying under vacuum overnight. Fourier transform infrared (FTIR) and nuclear magnetic resonance (NMR) spectroscopy were utilized to confirm synthesis of HCA. ^{1}H NMR ($CdCl_3$): 1.05 ppm (m, HOCHCH_3, 9H), 1.2 ppm (m, -OCHCH_3, 3H), 2.2–2.6 ppm (m, -CH_2-, 12H), 3.6 ppm (m, HOCHCH_3, 3H), 5.1 ppm (m, -OCHCH_3, 1H), 6.4 ppm (d, -CCH=, 1H), 7.3–7.6 ppm (m, -HC=CHC$_6H_5$, 6H).

SMP Foam and Film Synthesis

SMP foams were synthesized using the procedure described by Singhal et al.[27] Briefly, an isocyanate (NCO) pre-polymer was synthesized with appropriate molar ratios of HPED, triethanolamine (TEA), HCA or CA, and hexamethylene diisocyanate (HDI), with a 42 mol% hydroxyl (OH) content. A OH mixture was prepared with the remaining molar equivalents of HPED, TEA, and HCA or CA. Foaming agents (catalysts, surfactants, deionized water, and Enovate) were mixed with the NCO pre-polymer and the OH mixture using a speed mixer (FlackTek, Inc., Landrum, SC) to induce foam blowing. The foams were then cured at 50 °C for 5–10 min and cooled to room temperature before washing via sonication in isopropyl alcohol (IPA) or reverse osmosis (RO) water for 15 min cycles. The purified foams were lyophilized to dry.

SMP films were synthesized using the same monomer compositions as the foams, but without surfactants, deionized water, or Enovate. Table 1 shows the SMP compositions that were synthesized and characterized in these studies.

Table 1. Antimicrobial SMP compositions. NCO: isocyanate; OH: hydroxyl.

Formulation name	NCO equivalents [%] HDI	OH equivalents [%] HPED	TEA	CA	HCA
control	100	70	30	–	–
10% CA	100	70	20	10	–
10% HCA	100	70	20	–	10
20% HCA	100	70	10	–	20
30% HCA	100	70	–	–	30

SMP Foam Density

SMP foam density (n=3) was quantified on foam blocks cut from the top, middle, and bottom section of the foam, according to ASTM standard D-3574. Foam block masses was measured using a gravimetric scale, and length, width, and height values were measured three times per sample using a digital caliper. Density was calculated as mass divided by volume.

SMP Foam Pore Size and Structure

To assess pore sizes, thin slices (ca. 1 mm, n=3) were cut from each foam composition in the axial (parallel to foam rise) and transverse (perpendicular to foam rise) foaming directions. Samples were mounted to sample holders with carbon black tape and sputter-coated for 60 s at 20 mA (Cressington Sputter Coater, Ted Pella, Inc. Redding, CA). Samples were imaged using a Jeol NeoScope JCM-5000 Scanning Electron Microscope (SEM) (Nikon Instruments, Inc., Melviille, NY). A line was drawn through the center of each image, and pore size was measured for 5 randomly selected pores on the line using ImageJ software.

SMP Foam Thermal Transitions

The glass transition temperature (T_g) was measured under wet and dry conditions (n=5). To measure dry T_g, foam samples (3–8 mg) were cut and stored with desiccant prior to testing. A Q-200 DSC (TA Instruments, Inc., New Castle, DE) was used to obtain the thermogram for each composition using the following program: 1) temperature was decreased to −40 °C at 10 °C min^{-1} and held isothermally for 2 min, 2) temperature was increased to 120 °C at 10 °C min^{-1} and held isothermally for 2 min, 3) temperature was decreased to −40 °C at 10 °C min^{-1} and held isothermally for 2 min, and 4) temperature was increased to 120 °C at 10 °C min^{-1}. The dry T_g was recorded from the second heating cycle using the inflection point of the thermal transition curve. TA Instruments software (TA Instruments, Inc., New Castle, DE) was utilized to determine the inflection points.

For wet T_g measurements, foam samples (3–8 mg) were submerged in reverse osmosis (RO) water at 50 °C for 5 min to allow full plasticization. The samples were removed from the water, pressed dry with laboratory wipes, weighed, and placed in an aluminum pan with a vented aluminum lid. A Q-200 DSC was used to cool the samples to −40 °C at 10 °C min^{-1} and hold them isothermally for 2 min. The samples were then heated to 80 °C at 10 °C min^{-1}. TA instruments software was used to generate the thermogram and determine the wet T_g using the average inflection point of the thermal transition.

Volume Recovery

Cylindrical foam samples (n=3, diameter=4 mm, length=10 mm) were prepared, and a stabilizing 203.20 μm diameter nickel-titanium wire (NDC, Fremont, CA) was threaded through the center of each sample along its length. The foam samples were radially crimped to a 2 mm diameter using an ST 150-42 stent crimper (Machine Solutions, Flagstaff, AZ). Samples were heated to 100 °C, held isothermally for 15 min, and programmed to the crimped morphology by cooling to room temperature. Initial foam diameter was measured for each sample using Image J software (NIH, Bethesda, MD). The crimped foams were placed in a 37 °C water bath, and images were taken every 30 s up to 7 min. Foam diameter was measured at each time point at five evenly spaced locations along the foam length using Image J. Percent volume recovery was calculated using [Eq. (1)]:

$$\%\ \text{volume recovery} = \left(\frac{\text{recovered diameter}}{\text{original diameter}}\right)^2 * 100 \quad (1)$$

Cell Interactions

Human dermal fibroblasts (HDFs, Invitrogen, Inc., San Diego, CA) were used to assess cell attachment and spreading. *In vitro* culture was carried out at 37 °C/5% CO_2 with Medium 105 (Invitrogen) supplemented with low serum growth supplement (Invitrogen) and 1% penicillin-streptomycin (P/S, Gibco). Cells were used at passage 3.

SMP films were cut into 6 mm diameter cylinders and sterilized via incubation in 70% ethanol overnight and subsequent washing in sterile phosphate buffered saline (PBS, 3 washes). As a negative cell attachment control, wells in a 96 well tissue culture polystyrene (TCPS) plate were blocked with a sterile 5% bovine serum albumin (BSA) in PBS. Unmodified TCPS wells served as positive cell attachment controls. HDFs were seeded into wells containing SMP films at 5,000 cells cm^{-1}. Seeded cells were cultured at 37 °C/5% CO_2 for up to 72 h. Media was changed at 2 and 36 h. At 2 and 72 h, bright-field images were obtained to qualitatively assess cell attachment and proliferation. Representative images were obtained using a Nikon Eclipse TE2000-S with 4 field views per specimen and 3 specimens per sample type.

Antimicrobial Properties

To obtain an initial measure of antimicrobial properties, SMP films were cut into 6 mm diameter cylinders. To characterize antimicrobial properties over time, samples were incubated in PBS at 37 °C for 0, 10, 20, or 30 days. Then, films were sterilized as described in the Cell Interactions Section. *Escherichia coli* (*E. coli*) and *Staphylococcus epidermidis* (*Staph. epi.*) were grown overnight in 5 mL of lysogeny broth (LB) at 37 °C. Subsequently, 500 μL were taken from each overnight culture and grown in 10 mL of fresh LB to optical density (O.D.) 0.6 (i.e. until bacteria had entered log phase growth). O.D. was measured using a Tecan plate reader. Samples were placed into a sterile 96 well plate, and 100 μL of bacteria solution were pipetted onto the surface of each sample. Control SMP films were soaked in P/S overnight to provide a drug-based antimicrobial control. Samples were incubated with bacteria for 1 h at 37 °C and then vortexed to dislodge attached bacteria. Bacterial solutions were diluted by 10^6 in fresh LB and plated onto LB-agar plates overnight at 37 °C. Images were obtained of each specimen plating area. Colony forming unit (CFU) density was measured by counting the number of colonies and dividing by the plating area.

Statistics

Data are reported as mean ± standard deviation. Student's t-test was used to determine statistical significance, which was accepted at $p < 0.05$.

Keywords: antibiotics · phenolic acid · polymers · shape memory · synthesis design

[1] a) B. J. Eastridge, M. Hardin, J. Cantrell, L. Oetjen-Gerdes, T. Zubko, C. Mallak, C. E. Wade, J. Simmons, J. Mace, R. Mabry, R. Bolenbaucher, L. H. Blackbourne, *J. Trauma Acute Care Surg.* **2011**, *71*, S4 – S8; b) B. J. Eastridge, R. L. Mabry, P. Seguin, J. Cantrell, T. Tops, P. Uribe, O. Mallett, T. Zubko, L. Oetjen-Gerdes, T. E. Rasmussen, F. K. Butler, R. S. Kotwal, J. B. Holcomb, C. Wade, H. Champion, M. Lawnick, L. Moores, L. H. Blackbourne, *J. Trauma Acute Care Surg.* **2012**, *73*, S431 – S437; c) D. S. Kauvar, R. Lefering, C. E. Wade, *J. Trauma Acute Care Surg.* **2006**, *60*, S3 – S11; d) R. S. Kotwal, H. R. Montgomery, B. M. Kotwal, H. R. Champion, F. K. J. Butler, R. L. Mabry, J. S. Cain, L. H. Blackbourne, K. K. Mechler, J. B. Holcomb, *AMA Arch. Surg.* **2011**, *146*, 1350 – 1358.

[2] T. J. Walters, R. L. Mabry, *Mil. Med.* **2005**, *170*, 770 – 775.

[3] L. Dayan, C. Zinmann, S. Stahl, D. Norman, *Mil. Med.* **2008**, *173*, 63 – 66.

[4] A. E. Pusateri, H. E. Modrow, R. A. Harris, J. B. Holcomb, J. R. Hess, R. H. Mosebar, T. J. Reid, J. H. Nelson, C. W. Goodwin, Jr., G. M. Fitzpatrick, A. T. McManus, D. T. Zolock, J. L. Sondeen, R. L. Cornum, R. S. Martinez, *J. Trauma* **2003**, *55*, 518 – 526.

[5] G. R. Mueller, T. J. Pineda, H. X. Xie, J. S. Teach, A. D. Barofsky, J. R. Schmid, K. W. Gregory, *J. Trauma Acute Care Surg.* **2012**, *73*, S134 – S139.

[6] J. F. Kragh, Jr., J. K. Aden, J. Steinbaugh, M. Bullard, M. A. Dubick, *Am. J. Emerg. Med.* **2015**, *33*, 974 – 976.

[7] C. K. Murray, J. R. Hsu, J. S. Solomkin, J. J. Keeling, R. C. Andersen, J. R. Ficke, J. H. Calhoun, *J. Trauma Inj. Infect. Crit. Care* **2008**, *64*, S239 – S251.

[8] Y. S. Wong, A. V. Salvekar, K. D. Zhuang, H. Liu, W. R. Birch, K. H. Tay, W. M. Huang, S. S. Venkatraman, *Biomaterials* **2016**, *102*, 98 – 106.

[9] V. A. Kumar, N. C. Wickremasinghe, S. Shi, J. D. Hartgerink, *ACS Biomater. Sci. Eng.* **2015**, *1*, 1300 – 1305.

[10] A. Chaturvedi, M. B. Dowling, J. P. Gustin, T. M. Scalea, S. R. Raghavan, J. D. Pasley, M. Narayan, *J. Surg. Res.* **2017**, *207*, 45 – 52.

[11] B. B. Hsu, S. R. Hagerman, K. Jamieson, S. A. Castleberry, W. Wang, E. Holler, J. Y. Ljubimova, P. T. Hammond, *ACS Biomater. Sci. Eng.* **2015**, *1*, 148 – 156.

[12] A. Lendlein, S. Kelch, *Angew. Chem. Int. Ed.* **2002**, *41*, 2034 – 2057; *Angew. Chem.* **2002**, *114*, 2138 – 2162.

[13] A. Metcalfe, A.-C. Desfaits, I. Salazkin, L. H. Yahia, W. M. Sokolowski, J. Raymond, *Biomaterials* **2003**, *24*, 491 – 497.

[14] G. Ellson, M. Di Prima, T. Ware, X. Tang, W. Voit, *Smart Mater. Struct.* **2015**, *24*, 055001.

[15] D. Zhang, O. J. George, K. M. Petersen, A. C. Jimenez-Vergara, M. S. Hahn, M. A. Grunlan, *Acta Biomater.* **2014**, *10*, 4597 – 4605.

[16] T. S. Wilson, J. P. Bearinger, J. L. Herberg, J. E. Marion, W. J. Wright, C. L. Evans, D. J. Maitland, *J. Appl. Polym. Sci.* **2007**, *106*, 540 – 551.

[17] a) J. Horn, W. Hwang, S. L. Jessen, B. K. Keller, M. W. Miller, E. Tuzun, J. Hartman, F. J. Clubb, D. J. Maitland, *J. Biomed. Mater. Res. Part B* **2017**, *105*, 1892 – 1905; b) J. N. Rodriguez, F. J. Clubb, T. S. Wilson, M. W. Miller, T. W. Fossum, J. Hartman, E. Tuzun, P. Singhal, D. J. Maitland, *J. Biomed. Mater. Res. Part A* **2014**, *102*, 1231 – 1242.

[18] J. N. Rodriguez, M. W. Miller, A. Boyle, J. Horn, C.-K. Yang, T. S. Wilson, J. M. Ortega, W. Small, L. Nash, H. Skoog, D. J. Maitland, *J. Mech. Behav. Biomed. Mater.* **2014**, *40*, 102 – 114.

[19] a) A. J. Boyle, T. L. Landsman, M. A. Wierzbicki, L. D. Nash, W. Hwang, M. W. Miller, E. Tuzun, S. M. Hasan, D. J. Maitland, *J. Biomed. Mater. Res. Part B* **2015**, 104, 1407 – 1415; b) A. L. Nathan, W. Hwang, S. M. Herting, S. M. Hasan, M. B. B. Monroe, B. K. Keller, D. J. Maitland, *J. Med. Devices* **2016**, *11*, 011009-1.

[20] T. L. Landsman, T. Touchet, S. M. Hasan, C. Smith, B. Russell, J. Rivera, D. J. Maitland, E. M. Cosgriff-Hernandez, *Acta Biomater.* **2017**, *47*, 91 – 99.

[21] a) P. Singhal, W. Small, E. Cosgriff-Hernandez, D. J. Maitland, T. S. Wilson, *Acta Biomater.* **2014**, *10*, 67 – 76; b) L. Nash, M. Browning Monroe, Y.-H. Ding, K. Ezell, A. Boyle, R. Kadirvel, D. Kallmes, D. Maitland, *Polymers* **2017**, *9*, 381.

[22] K. S. Akers, K. Mende, K. A. Cheatle, W. C. Zera, X. Yu, M. L. Beckius, D. Aggarwal, P. Li, C. J. Sanchez, J. C. Wenke, A. C. Weintrob, D. R. Tribble, C. K. Murray, *BMC Infect. Dis.* **2014**, *14*, 1 – 11.

[23] M. L. Cohen, *Science* **1992**, *257*, 1050 – 1055.

[24] a) H. A. L. Wahdan, *Infection* **1998**, *26*, 26 – 31; b) R. Merkl, I. Hrádková, V. Filip, J. Šmidrkal, *Czech J. Food Sci.* **2010**, *28*, 275 – 279; c) G. G. F. Nascimento, J. Locatelli, P. C. Freitas, G. L. Silva, *Braz. J. Microbiol.* **2000**, *31*, 247 – 256.

[25] G. R. Teodoro, K. Ellepola, C. J. Seneviratne, C. Y. Koga-Ito, *Front. Microbiol.* **2015**, *6*, 1420.

[26] S. M. Fiuza, C. Gomes, L. J. Teixeira, M. T. Girão da Cruz, M. N. D. S. Cordeiro, N. Milhazes, F. Borges, M. P. M. Marques, *Bioorg. Med. Chem.* **2004**, *12*, 3581 – 3589.

[27] P. Singhal, J. N. Rodriguez, W. Small, S. Eagleston, J. Van de Water, D. J. Maitland, T. S. Wilson, *J. Polym. Sci. Part B* **2012**, *50*, 724 – 737.

[28] a) P. Singhal, A. Boyle, M. L. Brooks, S. Infanger, S. Letts, W. Small, D. J. Maitland, T. S. Wilson, *Macromol. Chem. Phys.* **2013**, *214*, 1204 – 1214; b) T. G. Rials, W. G. Glasser, *Holzforschung* **1984**, *38*, 191 – 199.

[29] A. C. Weems, A. Boyle, D. J. Maitland, *Smart Mater. Struct.* **2017**, *26*, 035054.

[30] T. Kheirbek, A. R. Kochanek, H. B. Alam, *Scand. J. Trauma, Resusc. Emerg. Med.* **2009**, *17*, 65 – 65.

[31] a) L. D. Nash, N. C. Docherty, M. B. B. Monroe, K. P. Ezell, J. K. Carrow, S. M. Hasan, A. K. Gaharwar, D. J. Maitland, *Macromol. Rapid Commun.* **2016**, *37*, 1945 – 1951; b) A. L. Nathan, G. K. Fletcher, M. B. B. Monroe, W. Hwang, S. M. Herting, S. M. Hasan, B. K. Keller, D. J. Maitland, *J. Med. Devices* **2017**, *11*, 011009.

[32] a) S. Tawata, S. Taira, N. Kobamoto, J. Zhu, M. Ishihara, S. Toyama, *Biosci. Biotechnol. Biochem.* **1996**, *60*, 909 – 910; b) B. Narasimhan, D. Belsare, D. Pharande, V. Mourya, A. Dhake, *Eur. J. Med. Chem.* **2004**, *39*, 827 – 834.
[33] F. Natella, M. Nardini, M. Di Felice, C. Scaccini, *J. Agric. Food Chem.* **1999**, *47*, 1453 – 1459.
[34] A. C. Weems, K. T. Wacker, J. K. Carrow, A. J. Boyle, D. J. Maitland, *Acta Biomater.* **2017**, *59*, 33 – 44.

Manuscript received: September 15, 2017
Accepted manuscript online: November 8, 2017
Version of record online: December 28, 2017